OXFORD

Cerebral Cortex, 2022, **32**, 4397–4421
https://doi.org/10.1093/cercor/bhab491
Advance access publication date 25 January 2022
Original Article

Modulation of pacemaker channel function in a model of thalamocortical hyperexcitability by demyelination and cytokines

Rahul Chaudhary[1], Stefanie Albrecht[2], Maia Datunashvili[1], Manuela Cerina[3], Annika Lüttjohann[1], Ye Han[4], Venu Narayanan[3], Dane M. Chetkovich[4], Tobias Ruck[5], Tanja Kuhlmann[2], Hans-Christian Pape[1], Sven G. Meuth[3,5], Mehrnoush Zobeiri[1,*,†], Thomas Budde[1,*,†]

[1]Institut für Physiologie I, Westfälische Wilhelms-Universität, 48149 Münster, Germany,
[2]Institute of Neuropathology, University Hospital Münster, 48149 Münster, Germany,
[3]Department of Neurology with Institute of Translational Neurology, Westfälische Wilhelms-Universität, 48149 Münster, Germany,
[4]Vanderbilt University Medical Center, Department of Neurology, Nashville, TN 37232, USA,
[5]Department of Neurology, Medical Faculty, Heinrich Heine University Düsseldorf, 40225 Düsseldorf, Germany
*Address correspondence to Dr Thomas Budde, Wilhelms-Universität, Institut für Physiologie I, Robert-Koch-Str. 27a, D-48149 Münster, Germany. Email: tbudde@uni-muenster.de; Dr Mehrnoush Zobeiri, Wilhelms-Universität, Institut für Physiologie I, Robert-Koch-Str. 27a, D-48149 Münster, Germany. Email: zobeiri@uni-muenster.de.
†Mehrnoush Zobeiri and Thomas Budde contributed equally to this study

A consensus is yet to be reached regarding the exact prevalence of epileptic seizures or epilepsy in multiple sclerosis (MS). In addition, the underlying pathophysiological basis of the reciprocal interaction among neuroinflammation, demyelination, and epilepsy remains unclear. Therefore, a better understanding of cellular and network mechanisms linking these pathologies is needed. Cuprizone-induced general demyelination in rodents is a valuable model for studying MS pathologies. Here, we studied the relationship among epileptic activity, loss of myelin, and pro-inflammatory cytokines by inducing acute, generalized demyelination in a genetic mouse model of human absence epilepsy, C3H/HeJ mice. Both cellular and network mechanisms were studied using in vivo and in vitro electrophysiological techniques. We found that acute, generalized demyelination in C3H/HeJ mice resulted in a lower number of spike–wave discharges, increased cortical theta oscillations, and reduction of slow rhythmic intrathalamic burst activity. In addition, generalized demyelination resulted in a significant reduction in the amplitude of the hyperpolarization-activated inward current (I_h) in thalamic relay cells, which was accompanied by lower surface expression of hyperpolarization-activated, cyclic nucleotide-gated channels, and the phosphorylated form of TRIP8b (pS237-TRIP8b). We suggest that demyelination-related changes in thalamic I_h may be one of the factors defining the prevalence of seizures in MS.

Key words: demyelination; epilepsy; HCN channels; SWDs; thalamocortical dysrhythmia.

Introduction

Multiple sclerosis (MS) is a complex, chronic neuroinflammatory disease of autoimmune origin, in which autoreactive lymphocytes induce neuroinflammation, myelin damage, and neurodegeneration (Filippi et al. 2018). The neuronal damage and altered neural signaling in MS result in a wide range of neurological symptoms that are determined by the location and the extent of the lesions. It is suggested that neuroinflammation and cortical lesions in MS are associated with an increased incidence of epilepsy and epileptic seizures; here, sclerosis may act as a focus for epileptic seizures (Calabrese et al. 2008). However, there is variability among current studies regarding the exact prevalence of seizures and the epilepsy in MS (Poser and Brinar 2003; Cano et al. 2021; Mirmosayyeb et al. 2021). A number of population-based cohort studies revealed a higher cumulative incidence of epilepsy and seizures in MS patients compared with the general population (Burman and Zelano 2017; Pack 2018; Neuß et al. 2020). Other studies have reported a smaller incidence of seizures and epilepsy, with a seizure sometimes representing the first neurological symptom of MS, with reoccurrence of seizures seeming to be dependent on the subtype of MS. Of note, recurrence was seen more often if the first seizure occurred simultaneously with an MS

Received: August 9, 2021. **Revised:** November 26, 2021. **Accepted:** November 28, 2021

relapse (Durmus et al. 2013; Kavčič and Hofmann 2017; Langenbruch et al. 2019). Nevertheless, there does seem to be consensus that seizures usually emerge early on in the disease (Kelley and Rodriguez 2009; Kavčič and Hofmann 2017; Langenbruch et al. 2019). Furthermore, there is a paucity of information regarding the effects of neuroinflammation and demyelination on a preexisting epileptic phenotype or established epilepsy. The question arises whether demyelination, axonal damage or neurodegeneration, the characteristics of MS, exacerbate already existing epileptic seizures? How is the neural network involved in epileptogenesis affected by MS? Finally, what are the underlying molecular and cellular mechanisms connecting these two pathologies? In the present study, we addressed several aspects of these questions by focusing on an animal model of a well-understood type of epilepsy involving the thalamocortical (TC) system, namely absence epilepsy (Meeren et al. 2002; van Luijtelaar and Zobeiri 2014). The TC system is the neuronal substrate for the generation and maintenance of synchronized rhythmic activity. Defined types of thalamic neurons possess intrinsic pacemaker properties and are synaptically interconnected in functional loops that facilitate recurrent physiological and pathophysiological oscillations. Here, members of the hyperpolarization-activated, cyclic nucleotide-gated (HCN) channel family exert major pacemaker function (He et al. 2014). In addition, HCN channels tightly control the excitability of thalamic and cortical neurons. Tetratricopeptide repeat containing Rab8b-interacting protein (TRIP8b) is an auxiliary subunit that regulates surface trafficking and function of HCN channels (Han et al. 2020). Oscillatory activity in the TC network is central to several neurocognitive functions (including perception and memory) during wakefulness and sleep. In addition, several apparently unrelated neurological and psychiatric conditions, including depression, neurogenic pain, and absence epilepsy, are characterized by the occurrence of slow resonant interactions between thalamus and cortex and have been termed TC dysrhythmia (TCD) syndromes (Llinás et al. 1999). Spike–wave discharges (SWDs) that have a focal cortical onset zone are the electrographic hallmark of absence seizures in humans and rodent epilepsy models. SWDs are generated as a result of pathological interactions within the TC system; specifically, in rat models of genetic absence epilepsy (genetic absence epilepsy rats from Strasbourg (GAERS) and Wistar Albino Glaxo rats bred in Rijswijk (WAG/Rij) rats) the sensory TC circuit is known to be involved in epileptogenesis (Meeren et al. 2002; van Luijtelaar and Zobeiri 2014). A number of gene mutations and transcriptional alterations in ligand- and voltage-gated ion channels have been identified in absence epilepsy families and TCD animal models (Crunelli et al. 2020). Especially, altered function of HCN1, HCN2, and HCN4 channels or their auxiliary subunit TRIP8b were associated with absence epilepsy and TCD in rats and mice (Ludwig et al. 2003; Ehling et al. 2012; Kanyshkova et al. 2012; Heuermann et al. 2016; Zobeiri et al. 2018; Zobeiri, van Luijtelaar, et al. 2019). In addition, GAERS and WAG/Rij rats revealed marked alterations in the density of parvalbumin-positive (PV^+) interneurons in different cortical and hippocampal regions (Papp et al. 2018; Arkan et al. 2019). Because C3H/HeJ mice have no other brain abnormalities, this strain has been suggested as a valid mouse model for studying idiopathic absence epilepsy (Frankel 2005). An insertion mutation in the Gria4 gene, encoding one of the four amino-3-hydroxy-5-methyl-4isoxazolepropionic acid (AMPA) receptor subunits in the brain, represents the major determinant of SWD generation in C3H/HeJ mice resulting in an early onset and fast postnatal maturation of SWD characteristics (Beyer et al. 2008; Ellens et al. 2009). The number of mature 7–8 Hz SWDs generated by these mice is rather moderate (average of 19 SWDs per hour), and an increased theta power during SWDs is found in the cortex and thalamus but not in the hippocampus.

Chronic demyelination is a valuable model for understanding mechanisms of demyelination-induced changes in subcortical sensory circuits and the generation of seizures in MS (Praet et al. 2014; Araújo et al. 2017; Lapato et al. 2017). Feeding mice with a diet containing 0.2% cuprizone mixed into a ground standard rodent chow for 5 weeks results in an acute, generalized demyelination (Skripuletz et al. 2008; Cerina et al. 2017, 2018, 2020). In cortical pyramidal cells, cuprizone treatment is associated with redistribution and altered expression of voltage-dependent Na^+ and K^+ channels (Rus et al. 2005; Hamada et al. 2016; Bozic et al. 2018). A longer period of cuprizone feeding (9–12 weeks) is associated with the appearance of hippocampal epileptic seizures; here pyramidal cell layer atrophy and loss of PV^+ interneurons, as well as changes in Aquaporin-4 expression, lead to development of seizures secondary to the demyelination (Lapato et al. 2017). To understand the effects of demyelination on an established epilepsy, in the current study, we induced acute, generalized demyelination in a genetic rodent model of human absence epilepsy, C3H/HeJ mice (Zendedel et al. 2013), using 0.2% of the copper chelator cuprizone for a period of 5 weeks. We then investigated the effects of acute demyelination followed by remyelination on the occurrence and characteristics of SWDs in C3H/HeJ mice. Although there are a number of studies demonstrating the complex time course of changes in cortical activity following cuprizone-induced demyelination (Ghaffarian et al. 2016; Cerina et al. 2017, 2018, 2020; Zhan et al. 2020), the effects of demyelination on thalamic activity are less investigated. In fact, only recently the critical role of the thalamus in neuroinflammatory diseases has been appreciated (Kipp et al. 2015). Thalamic atrophy and microstructural thalamic alterations are present in MS and are associated with damage to TC circuits (Kipp et al. 2012; Deppe et al. 2016). However, it is not clear how demyelination and neuroinflammation

affect intrathalamic network activity, physiological TC oscillations, and SWDs. By performing in vitro and in vivo field potential recording in the thalamus and cortex of cuprizone-treated C3H/HeJ mice, we determined the effects of demyelination and remyelination on intrathalamic network activity, as well as physiological and pathological oscillations using the TC network as neuronal substrate.

Numerous pro-inflammatory cytokines (including interleukin [IL]-1, IL-2, and IL-3) and interferons (IFNs, including IFN-α, IFN-β, and IFN-γ) released by microglia have been detected in demyelinating MS lesions (Zhao et al. 2013; Peferoen et al. 2014). Cuprizone-treated rodents showing general demyelination followed by remyelination revealed that Type I IFNs and IL-1β are released during the demyelination and remyelination phase, respectively (Plastini et al. 2020). It is reported that IL-1β and IL-6 can influence the passive and active membrane properties of TC neurons (Samios and Inoue 2014), yet the molecular substrates conveying these effects in TC cells and TC network are not, if at all, well investigated. Interestingly, pro-inflammatory cytokines like tumour necrosis factor (TNF)-α and IL-1β have been shown to increase the occurrence of SWDs in WAG/Rij rats, a genetic model of human absence epilepsy, further opening up the possibility that neurons of the TC network underlying SWD activity are modulated (Pinault and O'Brien 2005; Leresche et al. 2012; van Luijtelaar et al. 2012). To determine the effects of pro-inflammatory cytokines on thalamic cells and the TC network, we carried out in vitro electrophysiological experiments in the presence of different pro-inflammatory cytokines on control and cuprizone-treated C3H/HeJ mice. Based on the strong influence of HCN channels in TC network excitability and oscillations and the known redistribution of ion channels in the cuprizone model, we hypothesize that demyelination alters thalamic HCN channel function and consequently oscillatory activity in the TC system.

Here, we show that acute, generalized demyelination in epileptic C3H/HeJ mice results in lower numbers of SWDs, while theta frequency oscillations (interictal periods) increase during both sleep and wakefulness. We also show that demyelination in C3H/HeJ mice results in a significant reduction in thalamic rhythmic burst activity and lower amplitude of I_h. The reduction of I_h is accompanied by the reduced surface expression of HCN2, HCN4, and the phosphorylated form of TRIP8b (pS237-TRIP8b) in the thalamus.

Materials and Methods

Mice

All experiments were carried out in accordance with the European Committees Council Directive (2010/63/EU of the European Parliament) and were approved by the local authority (Landesamt für Natur, Umwelt und Verbraucherschutz). In this study, cuprizone-treated C3H/HeJ mice with acute, generalized demyelination were used as the experimental group and age and gender-matched non-treated C3H/HeJ mice (absence epilepsy model) were used as the control group. C3H/HeJ mice were bred in-house (ICB and Institute of Physiology I, Westfälische Wilhelms-Universität, Münster, Germany). All animals were kept under controlled environmental conditions (22–24 °C; 50–60% humidity; 12-h light/dark cycle).

Cuprizone Treatment

Male C3H/HeJ mice (6–8 weeks old) were subjected to cuprizone treatment through a diet containing 0.2% cuprizone in standard rodent chow for 5 weeks, during which time acute demyelination occurred (Cerina et al. 2017, 2018). Subsequently, normal chow was given to allow for spontaneous remyelination. Complete remyelination was attained on the 25th day following cessation of cuprizone feeding (Skripuletz et al. 2011). Recordings and staining were done on the 1st day (Day1, i.e., Day1 with normal chow/the day after stopping the cuprizone treatment), the 7th day (Day7), and the 25th day (Day25) of remyelination. Therefore, mice were between 3 and 4 months old when they were used in different experiments. Due to the relatively long duration of our in vivo local field potential (LFP) experiments (including the initial five weeks of cuprizone feeding), which could cause loss of LFP signal, control LFP recordings could not be performed on individual animals that were later treated with cuprizone. Therefore, age- and gender-matched C3H/HeJ mice were used as our control group.

In Vivo LFP Recording

Three to four months old male C3H/HeJ mice ($n = 5$) and cuprizone-treated C3H/HeJ mice ($n = 6$) were used as control and experimental groups, respectively. Implantation of the LFP recording electrodes, data collection, and signal analysis were performed as previously described (Zobeiri et al. 2018). Briefly, animals were anesthetized with an intraperitoneal (i.p.) injection of 50 mg/kg pentobarbital supplemented by a subcutaneous injection of Carprofen (Rimadyl; 5 mg/kg). The mouse head was fixed in a stereotactic frame (David Kopf Instruments, USA), and holes were drilled into the skull on top of the right hemisphere. Isolated (except at the tip) stainless steel wire recording electrodes (diameter 0.127 mm; impedance 500 KΩ, Franco Corradi, Milan, Italy) were inserted in the primary somatosensory cortex (S1; A/P = 0, M/L = 3, depth = −1.2) and two epidural silver wires were placed on top of the cerebellum to serve as ground and reference electrodes. The electrode assembly was fixed to the skull with the aid of dental acrylic cement. Following surgery, mice were single-housed and allowed to recover for at least one week. LFP signals were recorded continuously for 8 h during the light phase of the 12–12-h light–dark cycle (with lights on at 8 am). Recordings were performed in untreated control and cuprizone-treated C3H/HeJ mice on Days 1, 7, and 25 of remyelination

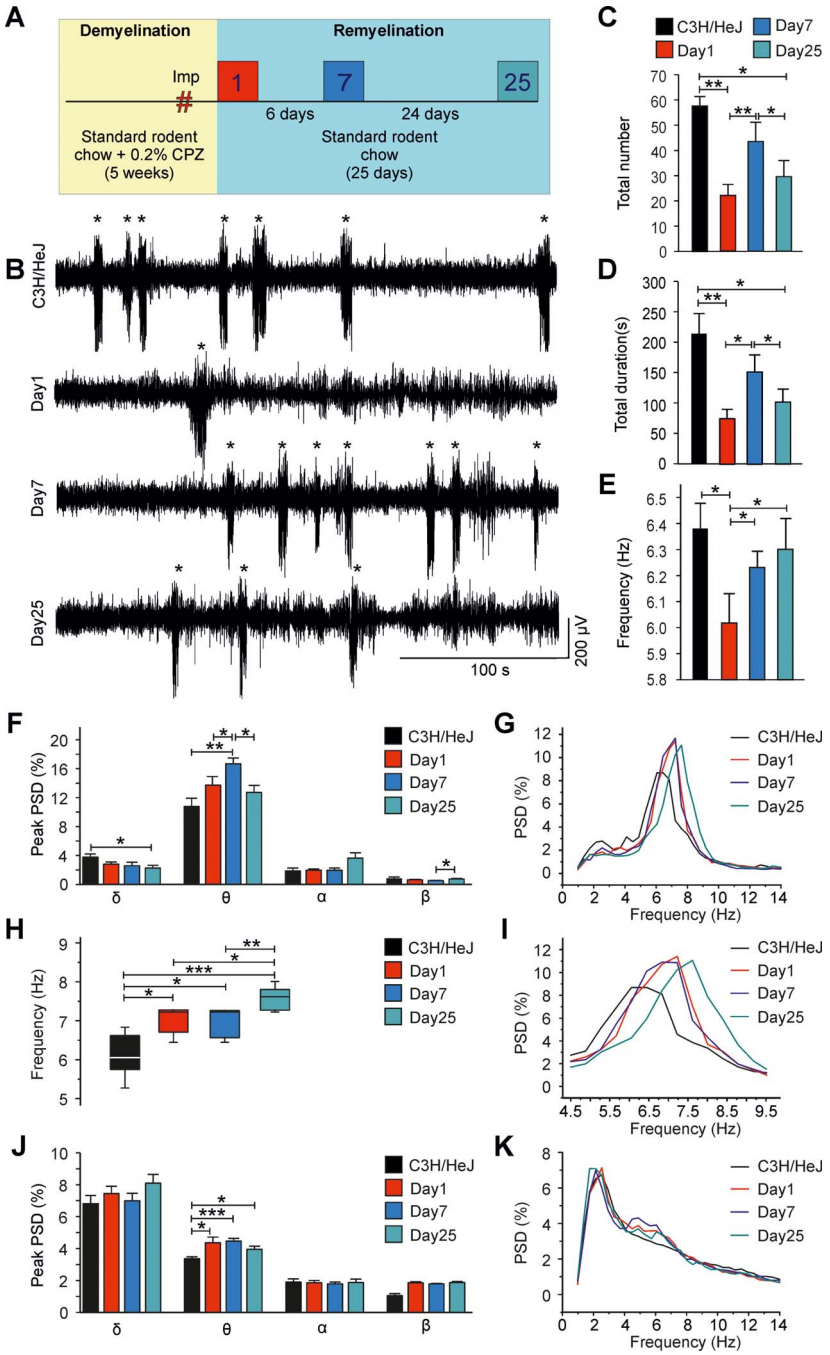

Fig. 1. Effects of general demyelination and remyelination on cortical oscillatory activity. (*A*) Schematic representation of the experimental paradigm including cuprizone (CPZ) feeding and days of in vivo LFP recording. C3H/HeJ mice were subjected to cuprizone treatment by giving a diet containing 0.2% cuprizone mixed into the standard rodent chow for 5 weeks causing the acute demyelination. Subsequently, normal chow was given to allow for spontaneous remyelination. LFP recordings were performed post-cuprizone treatment, on Days 1, 7, and 25. Complete remyelination was attained at the 25th day after stopping cuprizone feeding (see Fig. 2B and *D*). For convenience, days of LFP recordings are color coded. The red color represents Day1 of remyelination, which is immediately after stopping the cuprizone treatment, and the blue and green colors represent Days 7 and 25 of remyelination, respectively. Imp stands for electrode implantation. Recordings were performed during the light cycle for a period of 8 h (lights on 8 am). (*B*) Example LFP recording traces from somatosensory cortex (S1) illustrating the occurrence of SWDs (asterisks) in control epileptic C3H/HeJ mice and on Days 1, 7, and 25 of remyelination. (*C–E*) Bar graphs comparing the total number, total duration and frequency of SWDs (in 8 h of recording) between untreated control ($n = 5$) and cuprizone-treated C3H/HeJ mice ($n = 6$) on Days 1, 7, and 25 of remyelination. Repeated-measures ANOVAs were used for comparisons within cuprizone-treated group followed by Student's *t* tests as post hoc. Results were compared with untreated C3H/HeJ mice using Student's *t* tests. (*F*) Bar graph compares the normalized power spectral density (PSD in %) of peaks in delta (δ), theta (θ), alpha (α), and beta (β) bands during active-wakefulness between control epileptic C3H/HeJ mice and cuprizone-treated C3H/HeJ mice in different stages of remyelination. Only the first 2 h of light period were used for PSD analysis. (*G*) Representative spectrogram comparing the PSD% during active-wakefulness (average of 20 epochs of 2 s duration/animal) between control and cuprizone-treated C3H/HeJ mice. For clarity, only frequencies between 1 and 14 Hz are presented in this graph. As shown in (*G*), demyelination (Day1) followed by gradual remyelination (Days 7 and 25) is accompanied by a shift in theta band toward faster oscillations. (*H*) Boxplot illustrating the difference in the frequency of theta peak between control and cuprizone-treated C3H/HeJ mice. (*I*) Spectrogram illustrating changes in frequency of peak of theta indicated in (*G*). (*J*) Bar graph compares the PSD% of peak frequencies for delta, theta, alpha, and beta during slow-wave sleep (average of 20 epochs of 10 s duration/animal). (*K*) Comparison of the PSD% during slow-wave sleep between control and cuprizone-treated C3H/HeJ mice.

(Fig. 1A). Animals were connected to the recording set up via a cable and swivel allowing them to move freely during the recording. The LFP signals were amplified (Science Products DPA-2F), filtered by a band pass filter with cutoff points at 1 Hz (high pass) and 100 Hz (low pass) and digitalized with a constant sampling rate of 260 Hz by a CED recording system (Cambridge Electronic Design, UK). The behavioral activity of the animals was registered by a Passive Infrared Registration System (PIR, RK2000DPC LuNAR PR Ceiling Mount, Rokonet RISCO Group S.A., Belgium) placed on top of the registration box (van Luijtelaar et al. 2012). Following LPF recordings, animals were deeply anesthetized by isoflurane and brains were removed for histological verification of the correct electrode position. Offline analysis of recordings was carried out using NeuroExplorer 5 (Nex Technologies, USA) and Spike2 (version 7.08, Cambridge Electronic Design, UK) software. For analysis of interictal LFP, an offline band-pass filter (1–30 Hz) was additionally used for power spectral density (PSD) analysis. PSD was calculated for 75 bins covering the 1–30 Hz frequency range with a bin width of 0.4 Hz, for each individual animal, averaging the data from 20 epochs of 2 s for active wakefulness (AW) and 20 epochs of 10 s for deep slow-wave sleep (SWS). Epochs of AW and deep SWS were selected for each animal based on the LFP and PIR activity as previously described (Zobeiri et al. 2018). The non-REM sleep selection criteria included high-amplitude cortical electroencephalography (EEG) together with slow (1–5 Hz) waves in a motionless animal (as established by the PIR signal). AW criteria included behavioral activity (detected by high and variable PIR signal) accompanied by low-amplitude cortical EEG with theta and beta frequency oscillations. Only epochs from the first 2 h of the light period were selected; these hours represent the periods with the highest amount of specifically deep SWS (Huber et al. 2000). To control for individual differences in LFP amplitude, relative values (PSD %) were analyzed. Differences in PSD values between C3H/HeJ cuprizone-treated and C3H/HeJ control mice for each state of vigilance were evaluated by separate mixed-repeated-measure analyses of variance (ANOVAs) followed by post hoc Student's *t* tests (two sided).

SWDs were detected visually using common criteria including regular trains of sharp spikes and slow waves with the frequency of 5–8 Hz and spike amplitudes of at least twice the background LFP signal. Number, total duration, and intraspike frequency of SWDs were calculated for each animal over the period of 8 h and averaged in untreated control and cuprizone-treated (on Days 1, 7, and 25) C3H/HeJ mice.

Preparation of Acute Brain Slices for Ex Vivo Field Potential Recordings

Animals were sacrificed under deep isoflurane anesthesia and brain tissue was rapidly removed from the skull and placed in an ice-cold slicing solution containing (in mM): sucrose, 234; glucose, 11; NaH_2PO_4, 24; $MgSO_4$, 10; and $CaCl_2$, 0.5. This solution was equilibrated with a 95% O_2 and 5% CO_2 mixture. To preserve the intrathalamic connections between the thalamic reticular nucleus (TRN) and the ventrobasal complex (VB), horizontal brain slices of 400 μm thickness were obtained using a microtome (Leica VT 1200s, Leica, Wentzler, Germany) and incubated in artificial cerebrospinal fluid (ACSF; 32 °C) for 20 min and at room temperature (RT) for at least 1 h prior to recording. pH was adjusted to 7.35 by bubbling with carbogen (95% O_2 and 5% CO_2). In this preparation, the fiber bundles reaching from the internal capsule (IC) to VB were clearly visible.

Recording of Rhythmic Burst Activity in Slices

Horizontal slices were transferred to an interface chamber and recordings were performed at 32 ± 1 °C. The superfusion solution consisted of (in mM): NaCl, 126; KCl, 2.5; $NaHCO_3$, 26; NaH_2PO_4, 1.25; $MgCl_2$, 1; $CaCl_2$, 2; and glucose, 10. Rhythmic burst activity in the VB was evoked through stimulation of the IC using a 50–100 MΩ bipolar tungsten electrode. The stimulation electrode was connected to a custom-made amplifier and a stimulus isolator, and stimulus duration was controlled by WinLTPd101 software (WinLTP Ltd, University of Bristol, UK). Rhythmic burst activity was measured in the VB using a glass electrode (GC150T-10; Clark Electromedical Instruments, Pangbourne, UK) with a resistance of 0.5–2 MΩ. The stimulus consisted of one pulse (1.45 mA, 1 ms). Bursting was defined by at least three high-frequency spikes with an intra-burst frequency of >100 Hz and an inter-burst interval of <500 ms. Activity was measured and analyzed from 50 to 100 ms after the stimulation of IC for up to 2–3 s. All analyses were performed offline using Clampfit 10.7 (Molecular Devices, USA) and Peak v1.0 (Meuth IT Consulting, Germany) software.

Preparation of Acute Brain Slices for Patch-Clamp Recordings

Animals were sacrificed under deep isoflurane anesthesia and brain tissue was rapidly removed from the skull. Brain slices (250–300 μm) were prepared as coronal sections from untreated control and cuprizone-treated C3H/HeJ mice using ice-cold oxygenated slicing solution containing (in mM): sucrose, 200; PIPES, 20; KCl, 2.5; NaH_2PO_4, 1.25; $MgSO_4$, 10; $CaCl_2$, 0.5; dextrose, 10, pH 7.35 with NaOH. Before electrophysiological recordings, slices were transferred and kept in a chamber with ACSF (content in mM: NaCl, 120; KCl, 2.5; NaH_2PO_4, 1.25; $NaHCO_3$, 22; $MgSO_4$, 2; $CaCl_2$, 2; glucose, 25) at 32 °C for 20 min. Thereafter, slices were allowed to cool down to RT. pH was adjusted to 7.35 by bubbling with carbogen (95% O_2 and 5% CO_2).

Whole-Cell Voltage-Clamp Recordings in Acute Brain Slices

I_h was characterized by whole-cell voltage-clamp recordings from TC neurons of the VB region. Recording were carried out in an external solution (bath solution)

containing (in mM): NaCl, 125; KCl, 2.5; NaH_2PO_4, 1.25; HEPES, 30; $MgSO_4$, 2; $CaCl_2$, 2; Glucose10, 10; $BaCl_2$, 0.5–1 (only added in voltage-clamp recordings). pH was 7.25, at 30 ± 1 °C. Patch pipettes were pulled from borosilicate glass (GC150T-10; Clark Electromedical Instruments, Pangbourne, UK) and had resistances of 2.5–3.5 MΩ. The internal solution (pipette solution) contained the following (in mM): K-gluconate, 88; K_3-citrate, 20; NaCl, 10; HEPES, 10; $MgCl_2$, 1; $CaCl_2$, 0.5; BAPTA, 3; Mg-ATP, 3; Na_2-GTP, 0.5. The internal solution was set to a pH of 7.35 with KOH and an osmolality of 295 mOsmol/kg. All recordings were performed by patching the soma of TC neurons and using an EPC-10 amplifier (HEKA Elektronik, Lamprecht, Germany). The access resistance was in the range of 5–25 MΩ and was monitored throughout the whole experiment. Cells with access resistance of more than 25 MΩ were discarded from the experiment. Series resistance compensation of >40% was routinely applied. Voltage-clamp experiments were controlled by the software PatchMaster (HEKA Elektronik) operating on an IBM-compatible personal computer. All measurements were corrected for a liquid junction potential of 10 mV.

I_h current was measured by applying hyperpolarizing steps of −10 mV increment from a holding potential of −40 to −130 mV. The voltage protocol used to examine I_h was designed to increase the stability of whole-cell recordings and account for the increasingly fast activation kinetics of the current (Kanyshkova et al. 2012). Therefore, the pulse length was shortened by 500 ms with increasing hyperpolarization (3.5 s pulse length at −130 mV). Steady-state activation of I_h, P (V), was estimated by normalizing the mean tail current amplitudes (I) 50–100 ms after stepping to a constant potential from a variable amplitude step using the following equation:

$$P(V) = (I - I_{min}) / (I_{max} - I_{min}) \quad (1)$$

where I_{max} is the tail current amplitude for the voltage step from −130 to −100 mV and I_{min} represents the voltage step from −40 to −100 mV, respectively. I_h activation was fitted by the Boltzmann equation of the following form:

$$P(V) = 1/\left(1 + \exp\left((V - V_{0.5})/k\right)\right) \quad (2)$$

where $V_{0.5}$ represents the voltage of half-maximal activation and k the slope factor. The amplitude of I_h was calculated by subtracting the instantaneous current amplitude from the steady-state current. The density of I_h was calculated by dividing the I_h current amplitude at −130 mV by the membrane capacitance obtained during whole-cell recordings. The time course of I_h activation in TC neurons was best approximated by dual exponential equation as follows:

$$I_h(t) = A_0 + A_1\left(1 - \exp^{-t/\tau fast}\right) + A_2\left(1 - \exp^{-t/\tau slow}\right) \quad (3)$$

where $I_h(t)$ is the total amplitude of the current at time t; A_0 is the axis intercept; and A_1 and A_2 are the respective amplitudes of the components with fast (τfast) and slow (τslow) time constants.

Immunofluorescence

Mice were anesthetized by inhalation anesthesia (isoflurane, 5% in O_2; CP Pharma, Germany) and perfused transcardially with phosphate-buffered saline (PBS) and 4% paraformaldehyde (PFA). Brains were removed and post-fixed for 2 h in 4% PFA and later in 30% sucrose for 48–72 h. To facilitate delineation of the axonal fiber connections between IC and VB the horizontal orientation was chosen. Free-floating horizontal sections (40 μm) were cut and stored at −20 °C in cryoprotectant solution. Sections were washed three times for 10 min in PBS and incubated for 2 h in blocking solution (10% normal goat serum, 3% bovine serum albumin (BSA), 0.3% Triton-X100 in PBS) followed by 48 h of incubation at 4 °C with the following primary antibodies: polyclonal rabbit (rb)-anti-HCN2 (1:200), rb-anti-HCN4 (1:200; Alomone Labs), rb-anti-NeuN (neuronal specific marker, 1:1000; Abcam), mouse purified (ms)-anti-neurofilament marker (pan axonal, cocktail, SMI312; 1:200, BioLegend) and ms-anti-Parvalbumin (PV235, 1:500; Swant). After incubation with the primary antibodies, slices were washed three times for 10 min in PBS and thereafter transferred to the secondary antibody solution (Alexa Fluor 568 goat (gt)-anti-rb-IgG, 1:1000 and Alexa Fluor 488 gt-anti-ms-IgG, 1:500) for 2 h, washed three times for 10 min and mounted with a mounting medium (VECTASHIELD with 4′, 6-diamidino-2-phenylindole (DAPI), Vector Laboratories Inc., Burlingame, CA, USA) for confocal microscopy.

Staining of phosphorylated TRIP8b at residue 237 (pS237) was performed after antigen retrieval in 10 mM sodium citrate buffer, pH 9.0 for 10 min at 80 °C (Foote et al. 2019). Slices were then allowed to cool down for 1 h at RT and subsequently washed three times in 1 × PBST (1 × PBS with 0.3% Triton-X-100). Thereafter, slices were immersed in blocking solution (5% normal goat serum and 2% BSA in PBST) for another hour at RT and finally incubated overnight at 4 °C in primary antibodies (rb-α pS237; 1:100, YenZym, ms-anti-(constant) TRIP8b antibody (N212/7); 1:50, NeuroMab). After three washes in PBS, slices were transferred to the secondary antibody solution (Alexa Fluor 568 gt-anti-rb-IgG, 1:1000, Alexa Fluor 488 gt-anti-ms-IgG, 1:500) for 2 h and mounted with mounting medium containing DAPI.

For quantification of immunofluorescence staining, horizontal brain slices (average 2–3 slices/animal) containing the VB complex were visually detected. Stained slices were analyzed with a laser scanning confocal microscope (Nikon eC1 plus). The quantification of HCN2, HCN4, pS237, and TRIP8b was performed using ImageJ software (NIH) as integrated fluorescence intensity in regions of interest within the VB nucleus.

Quantitative Polymerase Chain Reaction

Dorsal thalamic, primary somatosensory cortical (S1) and hippocampal (HC) tissue was obtained from untreated

and cuprizone-treated C3H/HeJ mice and mechanically homogenized. RNA was then isolated using Trizol reagent (Invitrogen) following standard procedures. cDNA synthesis was performed using a standard protocol with random hexamer primers (Fermentas). Thereafter, cDNA was used to run quantitative polymerase chain reaction (qPCR) with fluorescein amidites-labeled Taqman primers (all from ThermoFisher Scientific) for IFN-β1 (Mm00439552_s1), IL-1β (Mm00434228_m1), TNF-α (Mm00443258_m1), IL-6 (Mm00446190_m1), and IFN-γ (Mm01168134_m1). 2′-Chloro-7′phenyl-1,4-dichloro-6-carboxy-fluorescein-labeled 18S rRNA was used as the endogenous control. qPCR was performed for 40 cycles and measured samples as duplicates from two independent experiments. Data were calculated using the change in cycle threshold ($\Delta Ct = Ct$ (gene of interest) – Ct (endogenous control)).

Histology

The brains of untreated control and cuprizone-treated C3H/HeJ mice (on Days 1, 7, and 25 of remyelination) were used for histological evaluation. The animals were sacrificed under deep isoflurane anesthesia by intracranial perfusion with PBS. Brains were removed and the hemispheres were cut sagittally in the midline. Both hemispheres were fixed in 4% (w/w) PFA solved in PBS overnight before embedding in paraffin. Sections (4 μm) were stained by luxol fast blue periodic acid schiff (LFB-PAS) solution for 72 h, washed with 0.05% Li_2CO_3 and subsequently stained with 1% periodic acid followed by Schiff reagent incubation for 20 min. Immunohistochemistry was performed using a biotin-streptavidin peroxidase technique (DAKO, K5001) and an automated immunostainer (Autostainer Link 48, DAKO). For better antigen retrieval, sections were pretreated with citrate buffer (pH 6) for 40 min in a steamer. After removing paraffin, intrinsic peroxidase was blocked by incubation with DAKO REAL™ Peroxidase Blocking solution (DAKO, S2023) for 5 min. All antibodies were diluted in DAKO REAL™ Antibody Diluent (DAKO, S0809) and sections were incubated (for 30 min at RT) with one of the following primary antibodies: rb-anti-NogoA (1:200; Millipore, AB5664P); rb-anti-Iba1 (1:500; Wako, 0199-19 741); ms-anti-CNPase (1:1000, BioLegend, 836 402); rb-anti-GFAP (1:4000, DAKO, Z0334), ms-anti-NeuN (1:100, Chemicon, MAB377). Thereafter, sections were incubated for 15 min at RT with secondary biotinylated anti-mouse/anti-rabbit antibody (DAKO, K5001). Nuclei counterstain was performed using DAKO REAL™ hematoxylin for 5 min at RT. DAKO REAL™ DAB+Chromogene (DAKO, K3468) was used as color substrate and sections were mounted with Eukitt® mounting medium (O. Kindler GmbH) after dehydration. LFB-PAS staining was quantified based on the gray value of myelin intensity whereas anti-NogoA, anti-Iba1, anti-CNPase anti-GFAP and anti-NeuN staining were quantified by determining the number of cells per mm^2.

Flow Cytometry

Flow cytometric analysis of murine peripheral leukocytes was performed as previously described (Ruck et al. 2013). For flow cytometric evaluation of central nervous system (CNS)-invading cells, mice were perfused transcardially with PBS. CNS tissue was dissociated mechanically, followed by an enzymatic digestion with collagenase, Type II (CLS-2) (Worthington) and DNase (Sigma Aldrich) for 45 min at 37 °C. After two washing steps, the cell suspension was transferred to a 30–50% Percoll (Amersham) density gradient. After centrifugation (2500 rpm, 30 min, 20 °C), mononuclear cells were isolated from the interface of the gradient, counted by a Casy® Model TT cell counter (Innovatis AG), to yield absolute cell numbers, and stained with appropriate antibodies. Calibrite beads were then added (BD Biosciences) to determine relative cell numbers as previously described (Bittner et al. 2017). The following primary anti-mouse antibodies were used for flow cytometry: CD3-Brilliant Violet 510 (clone 17A2); CD4-Phycoerythrin (clone GK1.5); CD8a-FITC (clone 53-6.7); CD11b-Pacific Blue (clone M1/70); CD11c-Allophycocyanin (clone N418); CD45-Allophycocyanin/Cy7 (clone 30-F11) (all purchased from BioLegend). Antibody concentrations were carefully titrated prior to experimentation. Cells were analyzed on a Gallios Flow Cytometer (Beckman Coulter, Krefeld, Germany).

Mathematical Modeling

Simulations were conducted within the NEURON simulation environment (Hines and Carnevale 2001; Meuth et al. 2005) based on a modified version of an intrathalamic network model consisting of four cells (Destexhe et al. 1996, 1998). The four-cell model comprised two spontaneously pacemaking TC neurons and two TRN neurons interacting via $GABA_A$, $GABA_{A/B}$, and AMPA synapses (see Fig. 5A). While TRN neuron parameters were not changed, the I_h modules of both TC neurons were modified by introducing $V_{0.5}$, activation kinetics and conductance values obtained by voltage-clamp recordings in C3H/HeJ, cuprizone-treated C3H/HeJ and C57BL/6J mice. In addition, an extended mathematical model was used to assess potential mechanisms for the decrease in SWDs seen on Day25 (Fig. 5B). Four different cell types were used for the eight-cell model (Destexhe et al. 1998), namely two cortical pyramidal neurons (PY), two cortical interneurons (IN), two TC neurons and two TRN neurons. As in the four-cell model, I_h parameters obtained from voltage-clamp recordings in TC neurons were used in an eight-cell simulation of network activity.

Drugs

Mouse IL-1β was purchased from Miltenyi Biotech (Bergisch Gladbach, Germany). The peptide was dissolved in deionized sterile-filtered water and aliquots were stored at −20 °C. The final concentrations used were 1.4 nM (IL-1β). Chinese-hamster-ovary-derived recombinant mouse

IFN-α from Hycultec GmbH (Beutelsbach, Germany) was used with a final concentration of 1000 IU ml^{-1}.

Statistical Analysis

All data are expressed as the mean ± standard error of the mean. Student's *t* tests were used for simple comparison between groups. In case of multiple comparisons, one-way or repeated-measures ANOVAs were used for analyses. Data were tested for normal distribution using the Kolmogorov–Smirnov test of normality. Mauchly's test of sphericity was used for the repeated-measures ANOVA. Where sphericity assumption was violated ($P < 0.05$), the Greenhouse–Geisser correction was applied. Student's *t* tests or Tukey honestly significant difference (HSD) test were used as post hoc tests. The data analysis was performed using IBM SPSS Statistic for Windows, Version 27.0 (Armonk, NY: IBM Corp.) and Origin (Pro), Version 2020b (OriginLab Corporation, Northampton, MA, USA). CorelDRAW Graphics Suite X8 was used for figure plotting. Differences were considered statistically significant if *P* values were <0.05; *, **, and *** indicate $P < 0.05$, $P < 0.01$, and $P < 0.001$, respectively.

Results

To assess the influence of demyelination on preexisting epilepsy, we induced acute, generalized demyelination in the CNS in a mouse model of absence epilepsy, C3H/HeJ, by targeting mature oligodendrocytes and feeding mice for 5 weeks with the copper chelator cuprizone (Skripuletz et al. 2011). Different electrophysiological, histological, and immunohistochemical readouts were obtained on three different time points (Days 1, 7, and 25) after stopping the cuprizone treatment (Fig. 1A), which are therefore referred to as Days 1, 7, and 25 of remyelination throughout the text. Results were compared to age- and gender-matched untreated C3H/HeJ mice.

Effect of Cuprizone Treatment on Cortical SWD Activity and TC Oscillations

To determine the possible impact of demyelination followed by remyelination on SWD generation, cortical LFPs were recorded from somatosensory cortex (S1) of cuprizone-treated C3H/HeJ mice ($n = 6$) on Days 1, 7, and 25 and were compared to untreated control group ($n = 5$). Under control conditions, C3H/HeJ mice showed frequent SWDs (Fig. 1B upper trace and Fig. 1C). A total number of 288 SWDs were analyzed in control C3H/HeJ mice ($n = 5$) over a period of 8 h recording. The mean number of SWDs/8 h of recording was 57.6 ± 7.5, with a total duration of 214.678 ± 34.56 s (Fig. 1C and *D*). The intra-SWD frequency was determined at 6.37 ± 0.1 Hz (Fig. 1E). Mice treated with cuprizone on Day1 ($n = 6$) showed a significant reduction in the total number (22.0 ± 4.34, df = 9, $t = 4.3$, $P = 0.002$), the total duration (74.7 ± 15.42 s, df = 9, $t = 3.9$, $P = 0.003$), and spike frequency (6.02 ± 0.1 Hz, df = 9, $t = 2.3$, $P = 0.034$) of SWDs as compared with untreated control C3H/HeJ mice (Fig. 1C–*E*). Compared to Day1, LFP recording of the animals on Day7 revealed a significant increase (repeated-measures ANOVAs with days of remyelination as the within-subject factor, followed by paired-sample *t* tests, $P < 0.05$) in all parameters, reaching values similar to C3H/HeJ control mice (total number of SWDs 43.43 ± 7.63, total duration of SWDs: 151.68 ± 28 s; frequency of SWDs: 6.23 ± 0.06 Hz; $n = 6$; Fig. 1C–*E*). However, on Day25 divergent results were obtained for the analyzed parameters. While the frequency of SWDs regained to control levels (6.3 ± 0.12 Hz), the number (29.4 ± 15.6), and total duration (101.9 ± 32.8 s) of SWDs decreased again ($n = 6$; Fig. 1C–*E*).

To understand the general impact of demyelination on physiological TC oscillations, we then compared the interictal activity of control and cuprizone-treated C3H/HeJ mice during two different behavioral states: AW (Fig. 1F–*I*) and SWS (Fig. 1*J* and *K*). Only frequencies between 1 and 30 Hz were used for PSD analysis. Comparing the normalized peak PSD (Peak PSD [%]) of delta (1–4.5 Hz), theta (4.5–8.5 Hz), alpha (8.5–12 Hz), and beta (12.5–30 Hz) frequency bands during AW between untreated control and cuprizone-treated C3H/HeJ mice on different days of remyelination (separate repeated-measures ANOVAs with four different frequencies as within-subject factors and groups as between-subject factors followed by Student's *t* tests), revealed a higher theta peak for Day1 (13.7 ± 2.6, $P > 0.05$) and Day7(16.9 ± 1.4, df = 9, $t = 4.4$, $P = 0.002$) and lower delta for Day25 (2.3 ± 0.9, df = 9, $t = 2.9$, $P = 0.03$) as compared with untreated control mice (C3H/HeJ control: theta: 10.8 ± 2.8 and delta: 3.8 ± 1.1). When Peak PSDs were compared between different days of remyelination within the cuprizone-treated group (repeated-measures ANOVAs with frequencies and days of remyelination as within-subject factors, followed by paired-sample *t* tests as post hoc), Day7 showed the highest peak for theta compared to Days 1 and 25 (Day7: 16.9 ± 1.4 vs. Day1: 13.7 ± 2.6, df = 4, $t = 3.9$, $P = 0.017$ and Day7: 16.9 ± 1.4 vs. Day25: 12.7 ± 2.1, df = 4, $t = 2.9$, $P = 0.044$), while the beta peak was higher on Day25 than on Day7 (Day25: 0.7 ± 0.2 vs. Day7: 0.5 ± 0.1, df = 4, $t = 3.7$, $P = 0.021$). Comparison of the PSD% of 1–30 Hz between control and cuprizone-treated C3H/HeJ mice showed a gradual shift in theta band toward faster oscillations during different stages of remyelination (Fig. 1G). This was demonstrated by a significant interaction for frequency and groups on Day1 ($F[74, 666] = 2.55$, $P = 0.000$), on Day7 ($F[74, 666] = 1.6$, $P = 0.001$) and on Day25 ($F[74, 666] = 6.7$, $P = 0.000$) and a significant main effect for groups on Day7 ($F[1, 9] = 5.5$, $P = 0.044$) and Day25 ($F[1, 9] = 8.6$, $P = 0.017$). Point-to-point comparison of different frequency values between the untreated and cuprizone-treated groups on different days of remyelination revealed significant differences in PSD% for frequencies between 6.8 and 8 Hz. In addition, comparing the PSD% of 1–30 Hz within the cuprizone-treated group demonstrated faster theta activity on Day25 compared with Days 1 and 7

($F[148, 592] = 1.74$, $P = 0.000$). Analysis of theta frequency peaks between control and cuprizone-treated group and within cuprizone-treated group showed an increasingly higher peak in the theta band frequency by the end of remyelination on Day25 (Fig. 1*H* and *I*).

Fewer changes were observed during SWS (Fig. 1*J* and *K*). Comparing the peak PSD of four different bands during SWS between the two groups revealed a higher theta peak for Day1 (4.4 ± 0.35, $P = 0.18$), Day7 (4.5 ± 0.17, $P = 0.000$) and Day25 (3.9 ± 0.2, $P = 0.03$) compared with untreated controls (1.9 ± 0.4, $P = 0.026$).

These findings revealed complex time-dependent alterations of epileptic activity following cuprizone treatment and changes in physiological TC oscillations, especially theta but also delta, during the course of demyelination and remyelination.

There is a clear relationship between the occurrence of SWDs and the state of vigilance (Coenen et al. 1991). To understand whether time-dependent alterations in epileptic activity following cuprizone treatment is associated with changes in behavioral states of the animals, we assessed effects of general demyelination and remyelination on sleep and wake periods of C3H/HeJ mice (Supplementary Fig. S1). Sleep–wake scorning was performed on the LFP data recorded during the first 8 h of light cycle (12:12-h light–dark cycle). The percentage of the time spent in wakefulness, rapid-eye movement (REM) and non-REM sleep were compared between untreated and cuprizone-treated C3H/HeJ mice on Days 1, 7, and 25 as well as within cuprizone-treated group during different days of demyelination/remyelination. No significant differences were found in hourly percentage of sleep and wake between untreated-control and cuprizone-treated mice (Supplementary Fig. S1A–C). Comparing the percentage of total time spent in each of the three states during 8 h of recording between untreated-control and cuprizone-treated mice revealed a statistically significant increase in the percentage of wakefulness on Day25 of remyelination as compared with untreated–control C3H/HeJ mice ($n = 6/5$ mice, $F[1,9] = 5.8$, $P < 0.05$, Supplementary Fig. S1*D*).

Reduced Rhythmic Burst Activity Following Demyelination

Intrathalamic network oscillations are involved in the generation of different thalamic rhythms, such as sleep spindle and delta waves, as well as pathological TC oscillation, such as occurring in different forms of absence epilepsy (Kanyshkova et al. 2009, 2012; Crunelli et al. 2014). Rhythmic bursting is a property of thalamic cells and has frequently been used as a measure of intrathalamic rhythmicity in horizontal thalamic slices conserving axonal connections between TRN and TC neurons in the VB (Huguenard and Prince 1994; Yue and Huguenard 2001). To understand the degree of demyelination of the IC (the main TC fiber tract) after cuprizone treatment, we quantified levels of myelin under different experimental conditions. LFB-PAS staining was performed and the intensity of staining in the IC was analyzed for different days of remyelination and compared with untreated control slices (Fig. 2*A*,*B*,*D*). There were statistically significant differences between untreated control and cuprizone-treated groups as determined by one-way ANOVA ($F[3, 28] = 31.3$, $P < 0.001$, $n = 4$ mice/group). Post hoc comparison using Tukey HSD test showed a significant decrease in the mean intensity of myelin in cuprizone-treated C3H/HeJ on Day1 (114.47 ± 7.25, $n = 8$ slices/4 mice, $P < 0.001$) and Day7 (147.50 ± 10.14, $n = 8$ slices/4 mice, $P < 0.001$) of remyelination compared with untreated control slices (195.20 ± 3.67, $n = 8$ slices/4 mice). The myelin intensity gradually increased (Day1 vs. Day7, $P < 0.05$; Day1 vs. Day25, $P < 0.001$; Day7 vs. Day25, $P < 0.001$) and finally returned to control values on Day25 (189.56 ± 3.91 Day25 vs. control, $P > 0.05$, see Fig. 2*D*). These results confirm the loss of myelin following cuprizone treatment and reveal regeneration of myelin sheaths after withdrawal of the cuprizone.

To understand how intrathalamic oscillations have been influenced by different degrees of demyelination, rhythmic burst activity was recorded in the VB in slices obtained from cuprizone-treated C3H/HeJ mice on Days 1, 7, and 25 and compared with untreated control slices (Fig. 2*C*, *E*–*G*, $n = 7$ mice/group). Compared with C3H/HeJ controls, thalamic slices prepared on Days 1 and 7 generated a significantly lower number of bursts in response to a single stimulation of the IC (Fig. 2*E*, 11.6 ± 0.67 for the control C3H/HeJ group versus 4.62 ± 0.29 on Day1 and 7.03 ± 0.75 on Day7, $n = 7$ mice/group, one-way ANOVA, $F[3, 24] = 34.6$, $P < 0.001$ followed by Tukey HSD test as post hoc, $Ps < 0.001$). The number of bursts was similar between control and Day25 (12.17 ± 0.65, $P > 0.05$). A gradual increase to control (i.e., baseline) values was observed when number of bursts was compared between different days of remyelination (Fig. 2*E*).

In accordance with the number of bursts, the summed duration of rhythmic bursts was also influenced by the degree of myelination (Fig. 2*F*). Slices from C3H/HeJ controls (1.61 ± 0.09 s) and Day25 (1.55 ± 0.06 s) showed longer bursting activity in comparison with Day1 (0.53 ± 0.03 s) and Day7 (0.88 ± 0.10 s, one-way ANOVA, $F[3, 24] = 46.8$, $P < 0.001$ followed by Tukey HSD test as post hoc, $Ps < 0.001$). Furthermore, the interburst frequency was significantly influenced by demyelination (one-way ANOVA, $F[3, 24] = 54.3$, $P < 0.001$ followed by Tukey HSD as post hoc). Bursts occurred more frequently in C3H/HeJ controls (6.82 ± 0.20 Hz) and at Day25 (6.99 ± 0.36 Hz) than at Day1 (2.93 ± 0.25 Hz, $Ps < 0.001$) and Day7 (4.41 ± 0.20 Hz, $P < 0.001$) (Fig. 2*G*).

These findings demonstrated that intrathalamic oscillations are strongly influenced by demyelination and that the incidence of burst firing is strongly correlated with the degree of myelination.

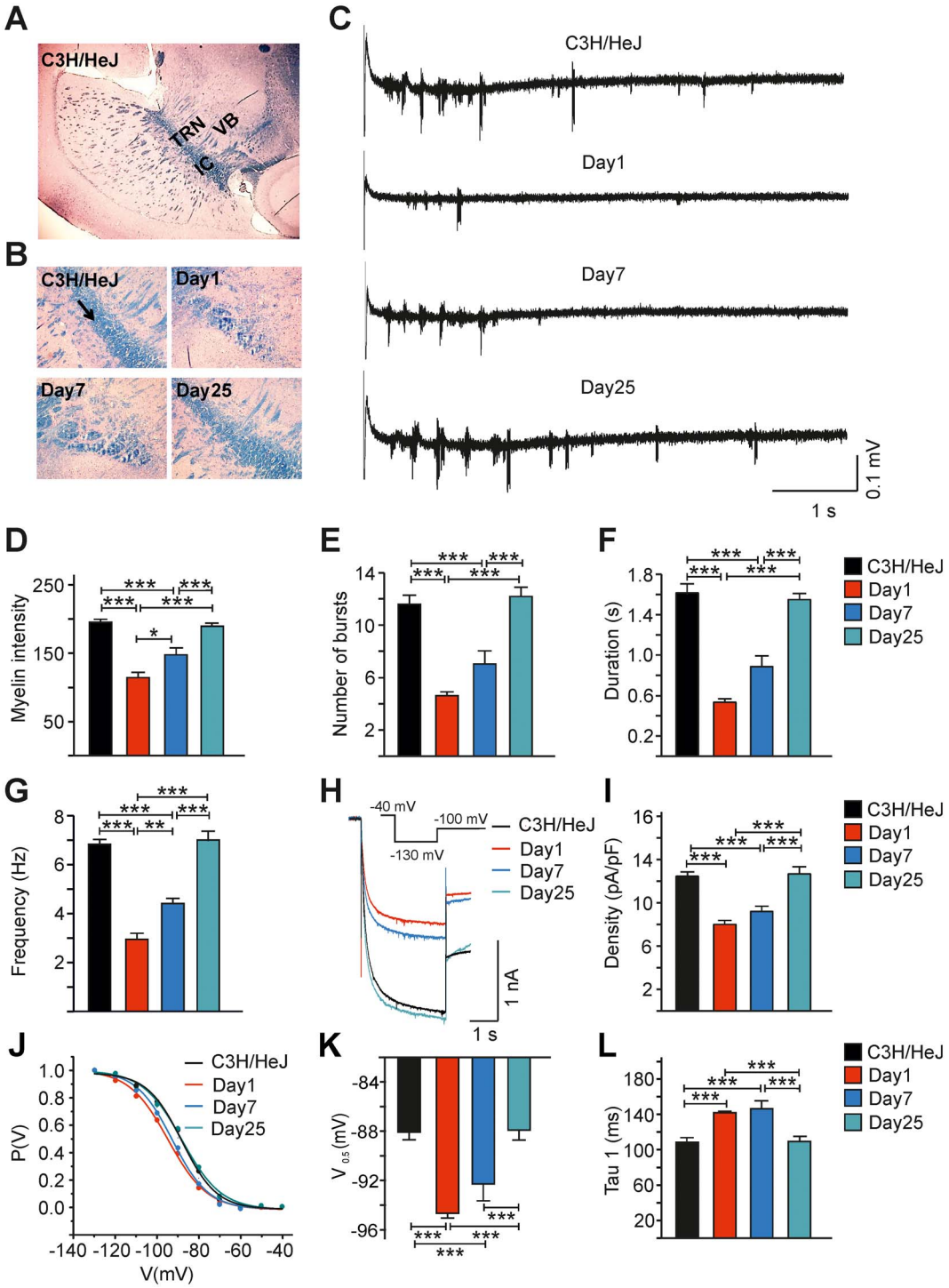

Fig. 2. Effects of general demyelination/remyelination on intrathalamic network activity and thalamic hyperpolarization-activated current. (*A*) Example LFB-PAS staining (×2.5 magnifications) which shows typical organization of myelin and thalamocortical connections in control C3H/HEJ mice (horizontal section, 400 μm). Here, IC, TRN, and VB stand for internal capsule, thalamic reticular nucleus and ventrobasal complex, respectively. (*B*) Example LFB-PAS stainings (×10 magnification) comparing the myelin intensity in IC (arrow head) between control C3H/HeJ and Days 1, 7, and 25 of remyelination. (*C*) Sample burst activity traces recorded from VB complex of control C3H/HeJ and cuprizone-treated C3H/HeJ mice during different stages of remyelination. Thalamic burst activity was recorded from the VB in horizontal brain slices (400 μm) and evoked by a single stimulation of the IC (1.45 mA, 1 ms). (*D*) Bar graph compares the intensity of the myelin obtained by LFB-PAS staining between control and cuprizone-treated groups. As shown in (*D*), the myelin intensity was significantly reduced on Day1 of remyelination in cuprizone-treated C3H/HEJ mice and gradually returned to control values by Day25. (*E–G*) Bar graphs comparing the mean number of bursts, the duration of bursts and interburst frequency in the VB between C3H/HEJ control and Days 1, 7, and 25 ($n = 7$ mice/group, 1–3 slices from each animal). As shown here, thalamic burst activity in the VB was dampened on Days 1 and 7 of remyelination and returned to the control values on Day25. (*H*) Sample traces of I_h recorded under voltage-clamp condition in TC neurons of the VB from control C3H/HEJ and cuprizone-treated C3H/HEJ mice in different remyelination stages. For clarity, only last hyperpolarizing steps (−130 mV, see also inset) are shown. (*I*) Bar graph compares the I_h density between control and cuprizone-treated VB neurons. (*J*) Mean steady-state activation curves of I_h from control C3H/HEJ and cuprizone-treated C3H/HEJ mice on Days 1, 7, and 25. (*K*) Comparison of the half-maximal activation ($V_{0.5}$) of I_h obtained from activation curves in *J* between C3H/HEJ control, Days 1, 7, and 25 of remyelination. (*L*) Bar graph compares the time constant of I_h activation (slow component, $\tau 1$) between control C3H/HeJ and cuprizone-treated VB cells on Days 1, 7, and 25.

Altered I_h Properties Following Demyelination

Cuprizone-treated C3H/HeJ mice showed prominent changes in low-frequency oscillations recorded in cortical LFP, the number and frequency of SWDs, as well as intrathalamic burst activity, thereby pointing to the possible modulation of some key generators of TC oscillation. Hyperpolarization-activated cation (HCN) channels modulate a number of cortical and thalamic rhythms, especially low-frequency oscillations (delta and theta) (Wahl-Schott and Biel 2009; He et al. 2014). Altered HCN channel function and availability has also been associated with an increase in slow TC oscillations (Datunashvili et al. 2018; Zobeiri et al. 2018; Zobeiri, Chaudhary, et al. 2019), as well as absence epilepsy (Ludwig et al. 2003; Budde et al. 2005; Kanyshkova et al. 2012). Therefore, we assessed basal hyperpolarization-activated current (I_h) characteristics ($V_{0.5}$, current density, activation time constants) in different experimental groups. I_h was recorded in TC neurons of VB using hyperpolarizing voltage steps of increasing amplitude and decreasing duration (Fig. 2*H* inset). Recordings were performed in control and cuprizone-treated C3H/HeJ mice on Days 1, 7, and 25 (Fig. 2*H*).

Analysis of the time-dependent inward current revealed a striking reduction in I_h amplitude following general demyelination (Fig. 2*H*). When current densities were compared (Fig. 2*I*), VB TC neurons in C3H/HeJ controls (12.44 ± 0.39 pA/pF) and on Day25 (12.66 ± 0.65 pA/pF) revealed higher values compared to Day1 (7.99 ± 0.37 pA/pF) and Day7 (9.19 ± 0.48 pA/pF) VB TC cells (Fig. 2*I*; one-way ANOVA, $F\,[3, 24] = 22.8$, $P < 0.001$, Tukey HSD as post hoc: control vs. Day1, $P < 0.001$; control vs. Day7, $P < 0.001$; Day1 vs. Day25, $P < 0.001$; Day7 vs. Day25, $P < 0.001$; $n = 7$ cells). In addition, the steady-state activation curve of I_h in VB TC neurons on Days 1 and 7 was shifted to more hyperpolarized potentials compared to C3H/HeJ controls and mice recorded on Day25 (Fig. 2*J* and *K*). Fitting the Boltzmann equation to the data points revealed $V_{0.5}$ values for controls (−88.06 ± 0.62 mV), Day1 (−94.65 ± 0.34 mV), Day7 (−92.28 ± 1.36 mV), and Day25 (−87.91 ± 0.79 mV) that were significantly different (one-way ANOVA, $F\,[3, 24] = 14.5$, $P < 0.001$, Tukey HSD as post hoc: control vs. Day1, $P < 0.001$; control vs. Day7, $P < 0.001$; Day1 vs. Day25, $P < 0.001$; Day7 vs. Day25, $P < 0.001$; $n = 7$ cells/group; Fig. 2*K*).

Next, the activation kinetic was determined for the current traces elicited by the pulse to −130 mV (Fig. 2*L*). Compared to C3H/HeJ controls (108.44 ± 3.61 ms) and Day25 (109.23 ± 3.67 ms), demyelination significantly slowed down the fast ($\tau 1$) component of I_h activation in mice on Day1 (141.77 ± 1.88 ms) and Day7 (146.32 ± 9.42 ms) (one-way ANOVA, $F\,[3, 24] = 14.02$, $P < 0.001$, Tukey HSD as post hoc: control vs. Day1, $P < 0.001$; control vs. Day7, $P < 0.001$; Day1 vs. Day25, $P < 0.001$; Day7 vs. Day25, $P < 0.001$; $n = 7$ cells) (Fig. 2*L*).

These findings revealed a demyelination-induced reduction and slowing of I_h that recovered to control values with remyelination and point to a possible influence of I_h availability on TC oscillations and the occurrence of SWDs.

HCN Channel and pS237-TRIP8b Protein Expression Following Cuprizone Treatment

Next, we determined whether alteration in I_h density and kinetics following cuprizone treatment is caused by changes in protein expression of HCN channels in the thalamus, specifically the HCN4 and HCN2 channels, the main thalamic isoforms (Ludwig et al. 2003; Zobeiri, Chaudhary, et al. 2019). HCN channel staining was compared with the protein expression of SMI312, a purified anti-neurofilament antibody (both middle and heavy neurofilament subunits), which serves as an axonal marker (Yuan et al. 2012). Compared with the control condition, on Day1 the immunohistochemical signals for SMI312, as well as both HCN2 and HCN4 channels were strongly reduced (Fig. 3*A–D*, separate one-way ANOVAs for SMI312: $F\,[3, 122] = 37.2$, $P < 0.001$, post hoc Tukey HSD, C3H/HeJ control vs. Day1: $P < 0.001$ and HCN2: $F\,[3, 122] = 46.9$, $P < 0.001$, post hoc Tukey HSD, C3H/HeJ control vs. Day1: $P < 0.001$ and for SMI312: $F\,[3, 78] = 30.7$, $P < 0.001$, post hoc Tukey HSD, C3H/HeJ control vs. Day1: $P < 0.001$ and HCN4: $F\,[3, 78] = 15.5$, $P < 0.001$, post hoc Tukey HSD, C3H/HeJ control vs. Day1; $P < 0.001$, $n = 4$ mice/group). Compared with Day1, on Days 7 and 25, the fluorescence signals for SMI312 and HCN4 increased again and reached control levels on Day25 (Supplementary Fig. S2*A–D*, post hoc Tukey HSD; $Ps < 0.05$). The immunohistochemical signal for HCN2 exceeded control levels from Day7 (post hoc Tukey HSD, control vs. Day7, $P < 0.05$, control vs. Day25, $P < 0.001$, Supplementary Fig. 2*B*).

The surface expression of HCN channels in VB TC neurons is closely regulated by the auxiliary subunit TRIP8b (Zobeiri et al. 2018). Therefore, we then assessed whether reduction of HCN2 and HCN4 channel surface expression in the thalamus following demyelination is associated with changes in TRIP8b or the phosphorylated form of TRIP8b (pS237) that shows enhanced binding to HCN channels (Foote et al. 2019). In accordance with the reduction in surface expression of HCN2 and HCN4 channels, on Day1 strong reduction in the fluorescence signal for pS237-TRIP8b (Fig. 3*E* and *F*, $df = 194$, $t = 3.5$, $P < 0.001$, $n = 6/6$ mice) was observed, while we found no changes in protein expression of total TRIP8b (Fig. 3*E* and *F*, $n = 3/3$ mice, $P > 0.05$).

These findings indicated a close correlation between changes in I_h current density and the degree of myelination. Strikingly, the approximate 34% reduction in I_h current density on Day1 was accompanied by very similar percentage reductions in HCN4 (33%) and pS237-TRIP8b (30%) expression.

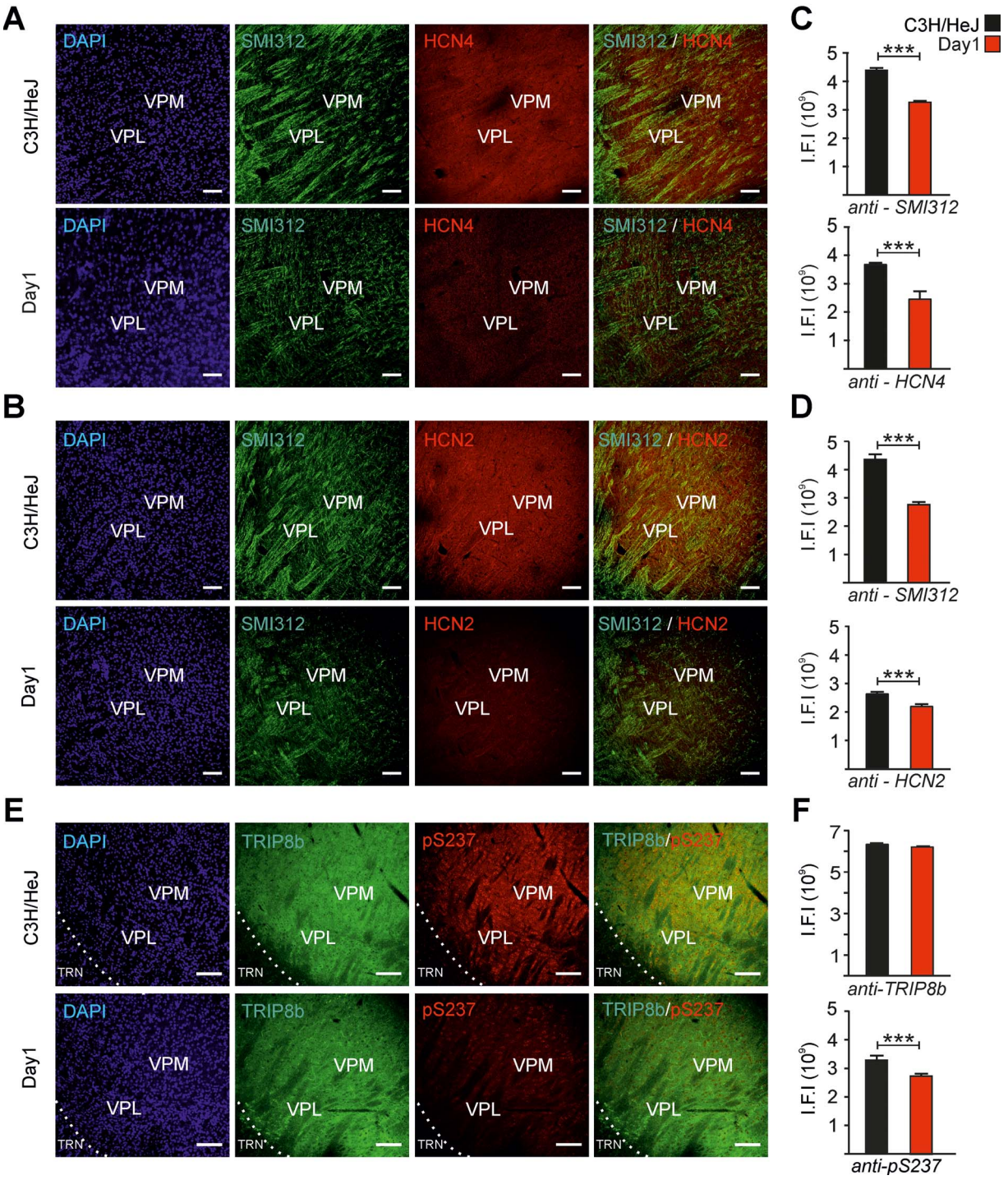

Fig. 3. Alteration in HCN channel expression in thalamus following general demyelination. (*A*,*B*) Immunofluorescence staining of the VB complex (horizontal thalamic sections, 40 μm) comparing the expression of HCN4 (A, in red, rb-anti-HCN4, 1:200, Alomone) and HCN2 (B, in red, rb-anti-HCN4, 1:200, Alomone) channels between control C3H/HeJ and Day1. The purified ms-anti- neurofilament antibody (SMI312, pan axonal, 1:200, BioLegend) was used as an axonal marker (SMI312, in green). Cell nuclei were stained with DAPI (in blue). (*C*,*D*) Bar graphs comparing the intensity of the fluorescence signal (using integrated fluorescence intensity values) for SMI312 (C and D upper traces) and HCN4 and HCN2 (lower traces) between the control C3H/HeJ and Day1. (*E*) Immunofluorescence staining of VB in control C3H/HeJ and Day1 with antibodies against TRIP8b (ms-anti-(constant) TRIP8b, 1:50, NeuroMab, in green) and phosphorylated TRIP8b (rb-α-pS237 antibody, 1:100, YenZym). (*F*) Representative bar graph comparing the intensity of the fluorescence signal for total TRIP8b and pS237 between the two groups indicating a significant reduction for phosphorylated TRIP8b, pS237, on Day1. Scale bars indicate 100 μm. VPL, VPM, and TRN stand for ventral-posterior medial, ventral-posterior lateral, and thalamic reticular nucleus, respectively.

Modulation of Rhythmic Burst Activity in Thalamic Network by Cytokines

Next, we determined the combined effect of myelination and cytokines, which are known to be released at different phases of demyelination and remyelination in the cuprizone model (Plastini et al. 2020). Therefore, intrathalamic burst activity was recorded before and after bath application of IFN-α and IL-1β (Fig. 4A and B), two pro-inflammatory cytokines that have been shown to influence TC cell activity (Samios and Inoue 2014). Application of IFN-α resulted in a significant reduction in the number (repeated-measures ANOVA, significant interaction for groups of experiment and number of bursts before and after application of IFN-α, $F[3, 20] = 7.91$, $P < 0.001$ and significant main effect for groups, $F[3, 20] = 28.22$, $P < 0.001$, $n = 6$ mice per group) and duration of bursts (repeated-measures ANOVA, significant interaction for groups of experiment and number of bursts before and after application of IFN-α, $F[3, 20] = 6.4$, $P < 0.001$ and significant main effect for groups, $F[3, 20] = 21.9$, $P < 0.001$) in both untreated (number of bursts in control: 11.53 ± 0.82 and in IFN-α: 7.85 ± 0.63, $n = 6$ mice, df = 5, $t = 6.7$, $P < 0.001$; duration of bursts in control: 1.56 ± 0.11 s and in IFN-α: 1.01 ± 0.11 s, $n = 6$ mice, df = 5, $t = 13.7$, $P < 0.001$) and cuprizone-treated C3H/HeJ mice on Day1 (number of bursts in control: 4.93 ± 0.24 and in IFN-α: 2.71 ± 0.31, $n = 6$ mice, df = 5, $t = 6.2$, $P < 0.01$; duration of bursts in control: 0.57 ± 0.09 s and in IFN-α: 0.41 ± 0.02 s, $n = 6$ mice, df = 5, $t = 2.9$, $P < 0.05$), Day7 (number of bursts in control: 6.18 ± 0.14 and IFN-α: 4.46 ± 0.24, $n = 6$ mice, df = 5, $t = 8.7$, $P < 0.001$; duration of bursts in control: 0.83 ± 0.08 s and in IFN-α: 0.46 ± 0.06 s, $n = 6$ mice, df = 5, $t = 5.7$, $P < 0.01$) and Day25 (number of bursts in control: 10.61 ± 0.73 and in IFN-α: 6.51 ± 0.57, $n = 6$ mice, df = 5, $t = 9.2$, $P < 0.001$; duration of bursts in control: 1.28 ± 0.10 s and IFN-α: 0.74 ± 0.08 s, $n = 6$ mice, df = 5, $t = 5.1$, $P < 0.01$) (Fig. 4C and E).

Application of IL-1β, on the other hand, significantly increased the number (Fig. 4D, repeated-measures ANOVA, significant interaction for groups of experiment and number of bursts before and after application of IL-1β, $F [3, 20] = 8.9$, $P < 0.001$ and significant main effect for groups, $F [3, 20] = 14.7$, $P < 0.001$) and duration of bursts (Fig. 4F, repeated-measures ANOVA significant interaction for groups of experiment and number of bursts before and after application of IL-1β, $F [3, 20] = 6.3$, $P < 0.001$ and significant main effect for groups, $F [3, 20] = 16.4$, $P < 0.001$) in untreated C3H/HeJ mice (number of bursts in control: 10.55 ± 1.00 and in IL-1β: 13.56 ± 0.77, $n = 6$ mice, student's t test as post hoc, df = 5, $t = 7.8$, $P < 0.001$; duration of bursts in control: 1.27 ± 0.12 s and in IL-1β: 2.04 ± 0.15 s, $n = 6$, df = 5, $t = 4.8$, $P < 0.01$), on Day7 (number of bursts in control: 7.51 ± 0.47 and in IL-1β: 9.74 ± 0.53, $n = 6$, student's t test as post hoc df = 5, $t = 3.6$, $P < 0.05$; duration of bursts in control: 0.85 ± 0.07 s and in IL-1β: 1.08 ± 0.07 s, $n = 6$ mice, df = 5, $t = 1.5$, $P < 0.05$) and on Day25 of remyelination (number of bursts in control: 12.22 ± 1.53, and in IL-1β: 15.62 ± 1.93, $n = 6$ mice, df = 5, $t = 7.2$, $P < 0.001$; duration of bursts in control: 1.55 ± 0.18 s and in IL-1β: 2.21 ± 0.29 s, $n = 6$ mice, df = 5, $t = 4.1$, $P < 0.01$) but had no effect on Day1.

These findings indicated that the two pro-inflammatory cytokines, IFN-α and IL-1β, differentially modulated intrathalamic oscillations.

Modulation of I_h Current in TC Neurons by Cytokines

Next, the combined effect of demyelination and cytokines on I_h was investigated. Voltage-clamp recordings were performed on TC VB cells of control and cuprizone-treated C3H/HeJ mice on Days 1, 7, and 25. I_h was recorded before and after bath application of IFN-α and IL-1β. Bath application of IFN-α decreased I_h density in both control and cuprizone-treated C3H/HeJ VB cells on different days of remyelination (Fig. 4G, left panel and Fig. 4H, lower panel, repeated-measures ANOVA, significant main effects for groups of experiment, $F [3, 20] = 10.6$, $P < 0.001$). Quantification revealed an IFN-α-induced reduction in I_h density in TC VB cells of untreated C3H/HeJ mice (Fig. 4H; control: 12.56 ± 0.51 pA/pF; IFN-α: 10.51 ± 0.52 pA/pF; $n = 6$ cells; df = 5, $t = 2.9$, $P < 0.05$) and cuprizone-treated TC VB cells on Day1 (control: 8.54 ± 0.59 pA/pF; IFN-α: 6.37 ± 0.81 pA/pF; $n = 6$ cells; df = 5, $t = 4.8$, $P < 0.01$) Day7 (control: 9.78 ± 0.47 pA/pF; IFN-α: 8.32 ± 0.30 pA/pF; $n = 6$ cells; df = 5, $t = 5.8$, $P < 0.01$) and Day25 (control: 12.10 ± 0.83 pA/pF; IFN-α: 10.01 ± 0.82 pA/pF, $n = 6$ cells; df = 5, $t = 3.4$, $P < 0.05$). Furthermore, IFN-α shifted voltage-dependent activation of I_h to more hyperpolarized potentials (Fig. 4H and $F [3, 20] = 71.2$, $P < 0.001$) in untreated C3H/HeJ mice: (control: -89.42 ± 0.71 mV; IFN-α: -93.43 ± 0.30 mV; $n = 6$ cells, df = 5, $t = 4.3$ $P < 0.01$), Day1 (control: -94.00 ± 1.70 mV; IFN-α: -96.56 ± 1.6 mV; $n = 6$ cells; df = 5, $t = 4.3$, $P < 0.01$), Day7 (control: -92.59 ± 1.75 mV; IFN-α: -95.38 ± 1.9 mV; $n = 6$ cells; df = 5, $t = 6.1$, $P < 0.01$), and Day25 (control: -89.32 ± 1.05 mV; IFN-α: -93.89 ± 0.96 mV; $n = 6$ cells; df = 5, $t = 3.9$, $P < 0.05$, Fig. 4H). When IL-1β was applied, a less uniform response was found (Fig. 4G–I). Current densities increased only in C3H/HeJ controls (control: 12.01 ± 0.47 pA/pF; IL-1β: 13.15 ± 0.72 pA/pF; $n = 6$ cells; student's t test as post hoc: df = 5, $t = 3.6$, $P < 0.05$) and on Day25 (control: 12.90 ± 1.08 pA/pF; IL-1β: 14.19 ± 1.04 pA/pF; $n = 6$ cells; post hoc: df = 5, $t = 4.04$, $P < 0.01$, Fig. 4I). Furthermore, IL-1β shifted the voltage-dependency of activation to more positive potentials in untreated C3H/HeJ mice (control: -89.25 ± 0.75 mV; IL-1β: -86.31 ± 1.19 mV; $n = 6$; student's t test as post hoc: df = 5, $t = 3.9$, $P < 0.01$) and on Day25 (control: -89.51 ± 0.62 mV; IL-1β: -86.67 ± 0.49 mV; $n = 6$; student's t test as post hoc: df = 5, $t = 9.9$, $P < 0.001$, Fig. 4I, upper panel). However, no significant effects were found on Days 1 and 7.

These findings indicate that IFN-α reduced I_h under basal and demyelinated conditions, while the activating effect of IL-1β was only visible during conditions of full myelination.

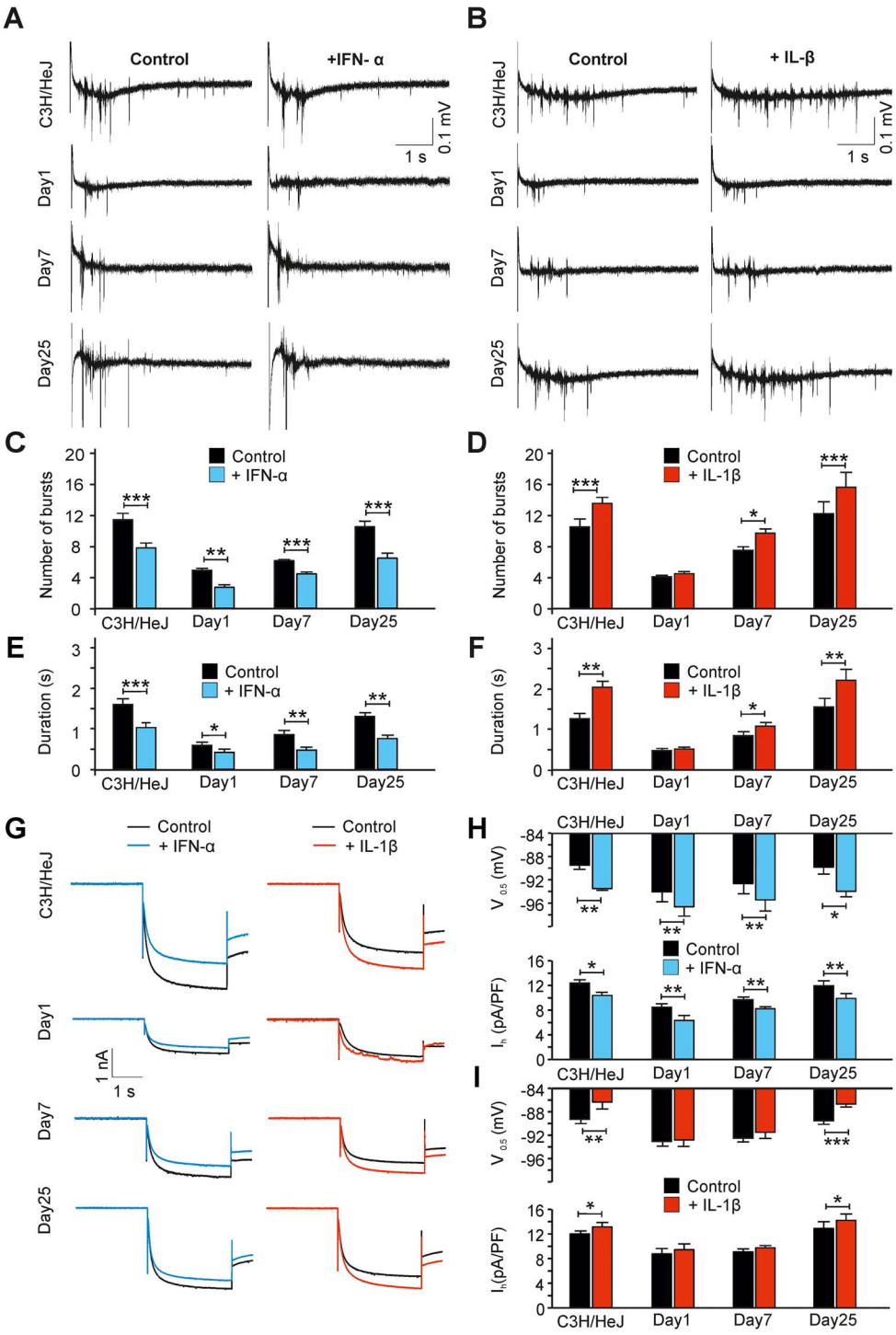

Fig. 4. Modulation of I_h in single TC neurons and thalamic network activity by cytokines. (*A*,*B*) Sample extracellular field potential recordings from VB complex demonstrating the modulatory effects of IFN-α (A) and IL-1β (*B*) on oscillatory burst activity in the thalamus of C3H/HEJ control and cuprizone-treated mice. Recordings were performed before (control) and 30 min after (+IFN-α or +IL-β) application of each substance. (*C*,*D*) Graphs indicate changes in the level of oscillatory burst activity after bath application of IFN-α (*C*) and IL-1β (*D*) in untreated control and cuprizone-treated C3H/HEJ mice in response to a single stimulus of the IC ($n = 6$ mice, 1–3 slices/animal/group). (*E*,*F*) Graphs compare the changes in the duration of oscillatory burst activity induced by IFN-α (*E*) and IL-1β (*F*) between C3H/HEJ control and C3H/HEJ cuprizone-treated mice ($n = 6$ mice, 1–3 slices/animal/group). (*G*) Sample I_h current traces recorded from VB TC neurons of C3H/HEJ control and C3H/HEJ cuprizone-treated mice before and after bath application of IFN-α (1000 IU mL^{-1}) and IL-1β (1.4 nM) illustrating the changes in the current amplitude. For clarity, only hyperpolarizing steps to −130 mV are shown. (*H*,*I*) Bar graphs compare effects of IFN-α and IL-1β on $V_{0.5}$ (H and I upper panels, $n = 6$ cells/group) and I_h current density (H and I, lower panels, $n = 6$ cells/group).

Mathematical Modeling of Intrathalamic Network Activity

By using a modified intrathalamic network model consisting of two TC and two TRN neurons interacting via $GABA_A$, $GABA_{A+B}$ and AMPA receptor synapses (Fig. 5A; Supplementary Fig. S4), we assessed how changes in I_h due to demyelination and remyelination and application of inflammatory cytokines influenced spontaneous rhythmic bursting. Specifically, intrathalamic network activity of the four-cell model was initiated by releasing the TC neurons from the RMPs observed during experiments and computed activity for three seconds. With the parameters for I_h conductance, $V_{0.5}$ and activation kinetics obtained from TC neurons of C3H/HeJ mice under different recording conditions, both TC neurons in the model generated spontaneous burst activity (Fig. 5C). A significantly higher number of bursts were generated by TC model neurons after using I_h parameters that were obtained from C3H/HeJ control mice (7.14 ± 0.55) and at Day25 (6.85 ± 0.4) compared to Day1 (1.42 ± 0.36) and Day7 (3.42 ± 0.52; one-way ANOVA, $F[3, 24] = 34.6$, $P < 0.001$, followed by Tukey HSD as post hoc: $Ps < 0.05$, Fig. 5E).

An extended mathematical model was used to assess potential mechanisms for the decrease in SWDs seen on Day25. In this model, two types of cortical neurons, including two pyramidal cells (PY) and two cortical interneurons (IN), were added to the thalamic four-cell model (Fig. 5B; Destexhe et al. 1998). Oscillations were evoked by electrical stimulation of one of the PY neurons (Fig. 5D, in blue). The parameters of I_h in TC neurons were set to the values as in the four-cell model, while the TRN and cortical neurons were unchanged. Under these conditions, the extended model largely corroborated the results of the thalamic model with respect to the number of rhythmic bursts. There was a significant decrease in the number of rhythmic bursts on Day1 (0.85 ± 0.14) and Day7 (2.14 ± 0.5) compared with untreated control condition (7.42 ± 0.57), and a gradual recovery to the control values occurred on Day25 (6.57 ± 0.68, $n = 7$, one-way ANOVA, F [4, 30] $= 31.1$, $P < 0.001$, post hoc Tukey HSD: $Ps < 0.05$) (Fig. 5D and F). As previous studies revealed an upregulation and redistribution of various K_V channels during MS-related inflammation (Rus et al. 2005; Bozic et al. 2018) and cuprizone-induced loss of myelin (Hamada and Kole 2015), we increased the conductance of the M-current module in both PY cells by 57% while using the experimental values for I_h in TC neurons as found at Day25. Under these conditions, the oscillatory activity of the extended model was strongly decreased (C3H/HeJ controls: 7.42 ± 0.57 vs. Day25 with increased M-current (I_M): 2.57 ± 0.52, $P < 0.001$; Day25 with normal M-current: 6.57 ± 0.68 vs. Day25 with increased I_M: 2.57 ± 0.52, $P < 0.01$) (Fig. 5F). This suggests that the decrease observed in the number of SWDs on Day25 of demyelination is potentially influenced by modulation of voltage-gated K_v channels in the cortex.

Next, I_h properties in TC neurons were set to model the combinations of I_h conductance, $V_{0.5}$ and activation kinetics observed during cytokine application on brain slices under different recording conditions using the four-cell model. In the presence of IFN-α, decreased bursting was found for C3H/HeJ controls (5.50 ± 0.56) and on Day1 (2.00 ± 1.63), Day7 (3.50 ± 2.25), and Day25 (4.50 ± 1.20, $n = 6$–7 trials, post hoc Tukey HSD: $Ps < 0.05$) (Supplementary Fig. S4). Parameters obtained during IL-1β application revealed increased bursting for C3H/HeJ controls (9.50 ± 0.43) and on Day1 (6.17 ± 0.65), Day7 (5.7 ± 1.61), and Day25 (9.33 ± 0.84) (all $n = 6$, post hoc Tukey HSD: $Ps < 0.05$) (Supplementary Fig. S4).

Overall, our findings indicate that, depending on the starting condition, both increases and decreases in I_h availability in TC neurons may result in reduced rhythmic intrathalamic activity.

Histological and Molecular Biological Evaluation

To further relate the electrophysiological findings to numbers of immunologically relevant cell types, immunohistochemical staining was performed on horizontal thalamic slices of C3H/HeJ control mice ($n = 4$) and C3H/HeJ ($n = 12$) mice treated with cuprizone. Assessments of astrocytes, microglia and oligodendrocytes were done using various markers (anti-CNPase, anti-Nogo A, anti-Iba1, anti-GFAP) (Fig. 6A and B). In addition, NeuN staining (Supplementary Fig. S3A–C) assessed the potential loss of neurons due to cuprizone treatment. Based on the finding that PV^+ neurons in the TRN are rhythmogenic, modulate somatosensory behavior and disrupt pharmacologically induced seizures, we also performed immunofluorescence staining of PV^+ neurons in thalamic slices (Supplementary Fig. S3A and B).

Reduction in the Number of Oligodendrocytes Following Demyelination

As oligodendrocytes are well known to be the main target of cuprizone treatment and are required for myelin sheath formation (Praet et al. 2014), anti-CNPase staining was performed. In comparison with C3H/HeJ controls (484.5 ± 26.36, $n = 4$ mice) and Day25 (501.02 ± 23.52, $n = 4$ mice), the staining showed a decrease in the number of oligodendrocytes in the IC on Day1 (332.25 ± 18.30, $n = 4$ mice, one-way ANOVA, F [3, 40] $= 17.4$ $P < 0.001$, post hoc Tukey HSD: $Ps < 0.001$) and Day7 (345.54 ± 16.13, $n = 4$ mice, one-way ANOVA, F [3, 40] $= 17.4$, post hoc Tukey HSD: $Ps < 0.001$). These findings confirmed that demyelination was based on the damage to oligodendrocytes due to cuprizone. In addition, cuprizone treatment resulted in a significant reduction in the number of mature oligodendrocyte (one-way ANOVA, F [3, 33] $= 6.7$, $P < 0.001$) in the IC on Day1 (338.74 ± 16.1, $n = 4$ mice, post hoc: $Ps < 0.01$,) and Day7 (315.95 ± 13.84, $n = 4$, mice, post hoc: $Ps < 0.01$) compared with C3H/HeJ controls (439.33 ± 27.64, $n = 4$ mice) and Day25 (426.90 ± 35.01, $n = 4$ mice) (Fig. 6A and B).

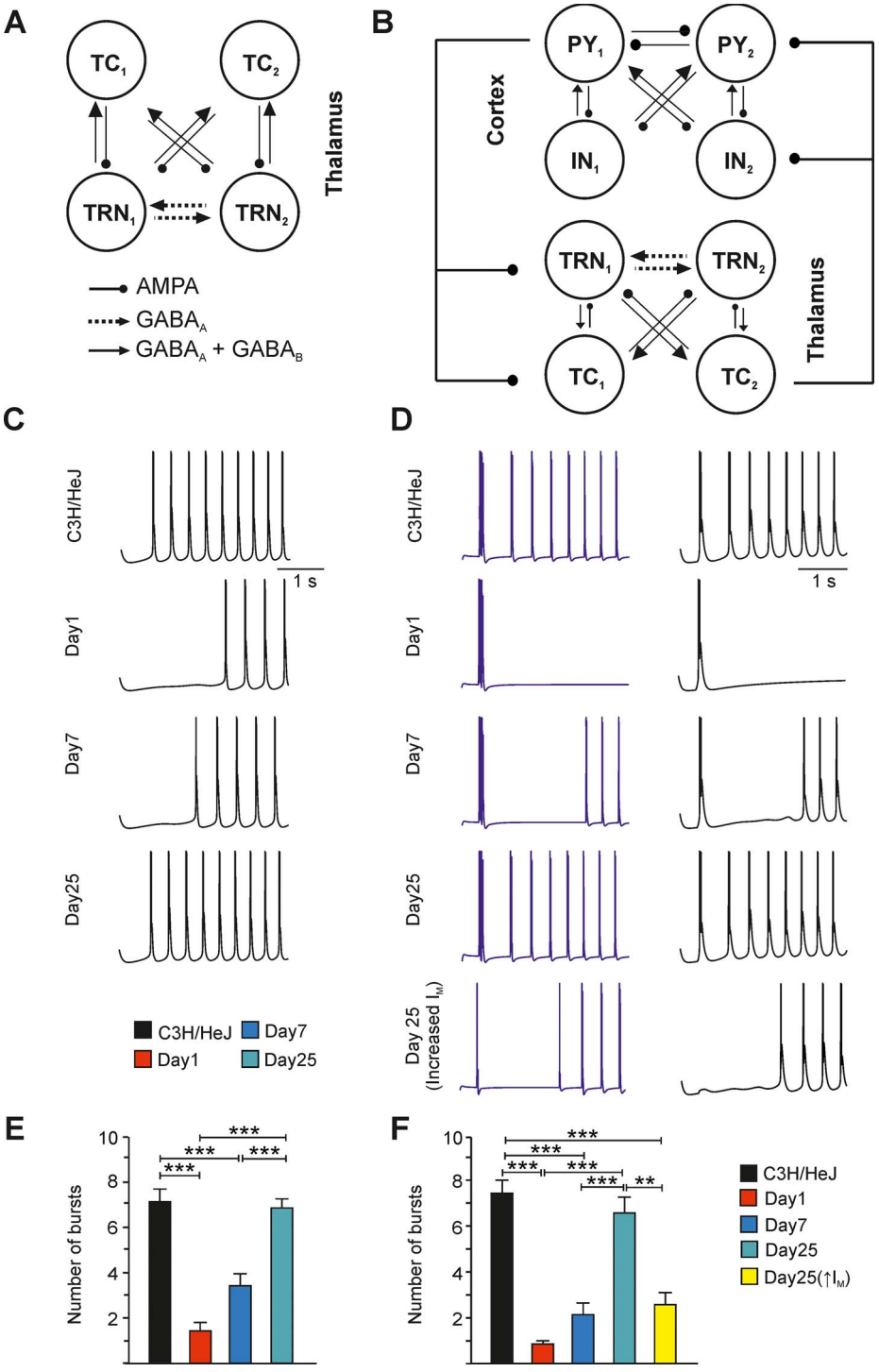

Fig. 5. Mathematical modeling of the intrathalamic and thalamocortical network activity before and following demyelination. (*A*,*B*) Mathematical modeling of intrathalamic and thalamocortical network activity using four-cell (*A*) and eight-cell (*B*) model systems, respectively. The network topology as well as the connection parameters corresponds to Destexhe (Destexhe et al. 1996, 1998). (*A*) In this intrathalamic four-cell model, $TRN_{1–2}$ (thalamic reticular neurons) neurons reciprocally communicate via $GABA_A$-mediated connections and project to both TC neurons via $GABA_A$ and $GABA_B$ signaling. The feedback from TC neurons is carried by AMPA receptors to both TRN cells. (*B*) In this eight-cell model, $PY_{1–2}$ (pyramidal) neurons of the cortex are connected to other neurons and to each other via AMPA receptor signaling. $IN_{1–2}$ (interneurons) of the cortex is connected to $PY_{1–2}$ neurons via $GABA_A$ and $GABA_B$ receptors. TRN (thalamic reticular neurons) neurons reciprocally communicate to each-other via $GABA_A$-mediated connections and project to both TC neurons via $GABA_A$ and $GABA_B$ signaling. The feedback from TC neurons is carried by AMPA receptors to both TRN and PY neurons. (*C*) Example traces obtained from intrathalamic four-cell model using I_h parameters recorded in vitro from VB cells of C3H/HeJ control and C3H/HeJ cuprizone-treated mice on Days 1, 7, and 25. (*D*) Example traces of the eight-cell model obtained by feeding the model with experimental values obtained from control and cuprizone-treated C3H/HeJ mice on Days 1, 7, and 25. Oscillations evoked by electrical stimulation of one pyramidal neuron (blue traces). Increase in the M-current (I_M, lowest panel in D) on Day25 of remyelination resulted in a decrease in the oscillatory activity of the model. (*E*) Bar graph compares the number of bursts generated by the intrathalamic four-cell model ($n = 7$ cells per group). (*F*) Bar graph compares the number of bursts in the VB generated by the intrathalamic eight-cell model. Comparisons were performed between control and cuprizone-treated C3H/HEJ mice on Days 1, 7, and 25 (with normal and increased I_M current).

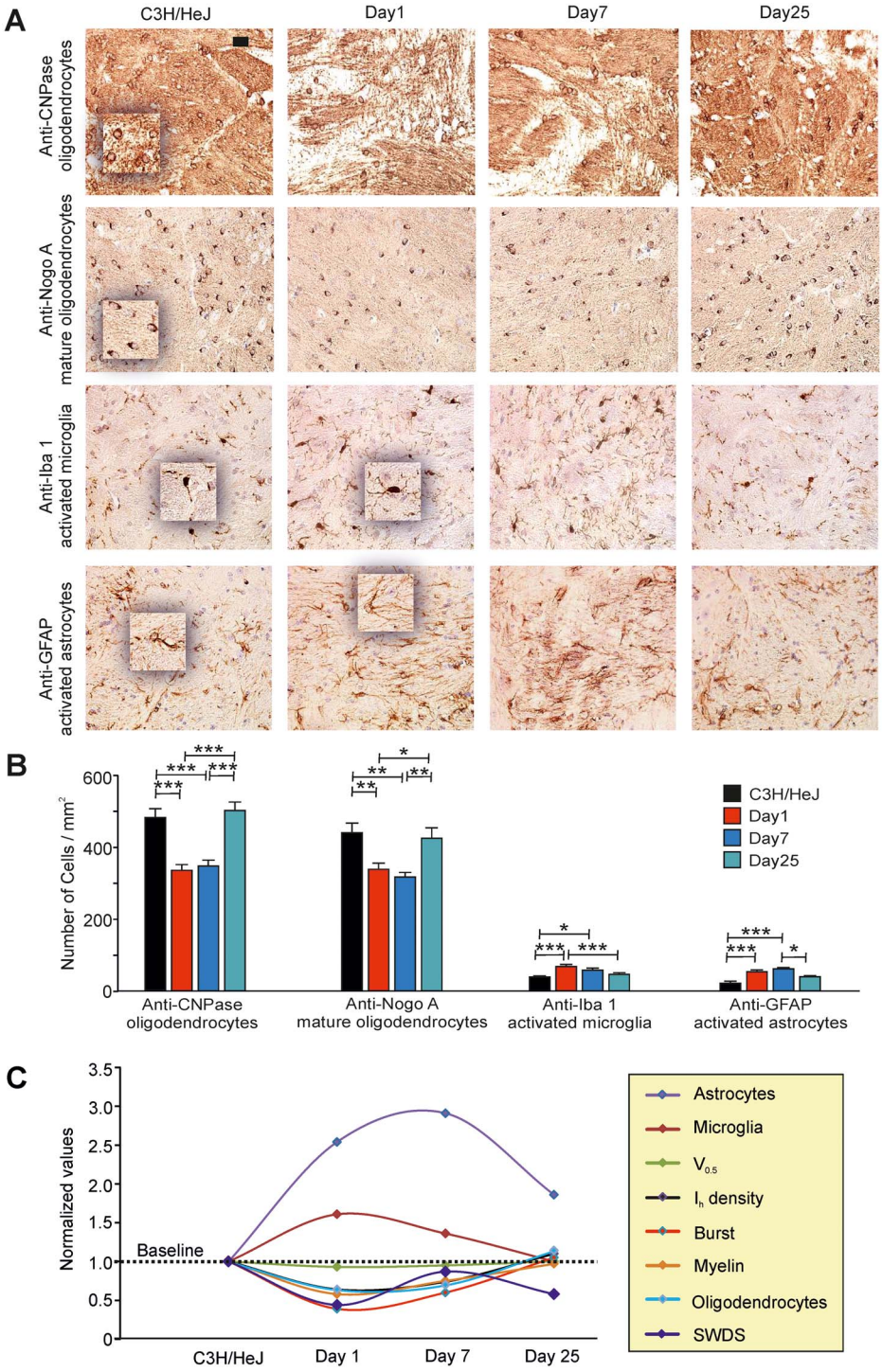

Fig. 6. General effects of de and remyelination on the cellular and electrophysiological parameters in epileptic C3H/HeJ mice. (*A*) Immunohistochemical staining of oligodendrocytes, microglia, and astrocytes in horizontal brain slices of untreated control and cuprizone-treated C3H/HEJ mice with anti-CNPase, anti-NOGO A, anti-Iba1, and anti-GFAP, respectively. Scale bar is 25 μm. Insets show cells in higher magnification. (*B*) Bar graph comparing the number of oligodendrocytes, mature oligodendrocytes, activated microglia, and activated astrocytes per mm^2 of IC between control and cuprizone-treated C3H/HEJ mice on Days 1, 7, and 25. (*C*) Diagram illustrating the relationship between normalized values of different parameters (indicated in the yellow box on the right side) plotted on the y-axis and different stages of demyelination/remyelination plotted on the x-axis. As shown in this figure, there is a significant increase in the number of activated astrocytes and microglia whereas $V_{0.5}$, I_h current density, rhythmic burst activity, myelin, oligodendrocytes, and SWDs are significantly decreased due to cuprizone-induced demyelination.

Demyelination Increased the Microglial and Astrocytes Activation

Microglial activation is a sign of brain inflammation and has been observed in previous studies to occur during cuprizone treatment (Hiremath et al. 1998; Graeber et al. 2011). Activated microglial cells were characterized by an amoeboid shape rather than spherical appearance (Cerina et al. 2017). In comparison to C3H/HeJ controls (38.51 ± 2.4) and Day25 (42.61 ± 3.62), staining showed an increase in the number of activated

microglia cells in the IC on Day1 (66.6 ± 4.44, one-way ANOVA, F [3, 42] = 9.6, $P < 0.001$, followed by Tukey HSD as post hoc: Ps < 0.01 for C3H/HeJ controls vs. Day1 and for Day1 vs. Day25, $n = 4$ mice per group) (Fig. 6B).

Astrogliosis is considered to be an important process during brain inflammation and is also known as a hallmark of cuprizone treatment (Hiremath et al. 1998; Colombo and Farina 2016). Activated astrocytes were differentiated from normal astrocytes based on their hypertrophy (Hiremath et al. 1998). In comparison to C3H/HeJ controls (20.76 ± 5.94) (Fig. 6A and B) staining showed a significant increase in the number of activated astrocytes (one-way ANOVA, F [3, 28] = 14.5, $P < 0.001$, $n = 4$ mice/group) in the IC on Day1 (52.80 ± 5.10, post hoc: $P < 0.001$) and Day7 (60.47 ± 3.66, post hoc: $P < 0.001$). The number of astrocytes on Day25 (38.81 ± 3.03) gradually returned to control values. Our results confirmed that cuprizone-induced demyelination caused astrocyte activation.

NeuN and PV Staining in Different Brain Regions

The number of NeuN-positive cells that represent mature neurons remained similar between C3H/HeJ control and cuprizone-treated mice in TRN (Supplementary Fig. S3A and B), the hippocampal CA1 region and neocortex (Supplementary Fig. S3C). In addition no differences in the number of PV^+ neurons were found in different TRN compartments on Day1 as compared with untreated-control C3H/HeJ (Supplementary Fig. S3A and B).

Cytokines and CNS-Invading Inflammatory Cells

Quantitative PCR of inflammatory cytokines and flow cytometry of immune cell distribution in the periphery and in the brain showed no relevant differences between C3H/HeJ controls and Day1 (Supplementary Figs S5 and S6). However, there was increased expression of TNF-α (C3H/HEJ controls: 28 ± 0.41, Day1: 26.20 ± 0.27, df = 6, $t = 4.8$, $P < 0.05$, $n = 4$ mice) and IL-6 (C3H/HEJ controls: 27.83 ± 0.33, Day1: 26.83 ± 0.12, df = 6, $t = 1.7$, $P < 0.05$, $n = 4$ mice) in the hippocampus on Day1. Of note, there were no significant changes observed in the expression of inflammatory cytokines in the thalamus and primary somatosensory cortex (S1).

The histological staining showed that, compared with C3H/HeJ controls and Day25, the amount of myelin and number of oligodendrocytes was significantly lower on Days 1 and 7, whereas microglia and astrocytes activation was higher on Days 1 and 7. Furthermore, we observed no relevant inflammatory responses following cuprizone as previously described (Cerina et al. 2017) and unchanged numbers of neurons in different brain regions.

Discussion

In the present study, we assessed the effects of different MS-related pathologies, namely general demyelination and pro-inflammatory cytokines, on epileptic seizures in the TC system, intrathalamic oscillations and HCN channel properties in TC neurons in a mouse model of absence epilepsy, C3H/HeJ. We found that the cuprizone-induced loss of myelin and oligodendrocytes in conjunction with the increase in activated microglia cells and astrocytes (on Day1) are associated with lower number of SWDs, increased theta frequency oscillations on cortical LFP, lower intrathalamic burst activity and finally reduced availability of I_h in TC neurons. Furthermore, the overall number of mature neurons was unchanged in TRN, neocortex and hippocampus on Day1, thereby indicating a lack of neurodegeneration. In addition, the number of PV^+ neurons in TRN remained unchanged. During the course of remyelination that lasted 25 days, all but two of the investigated parameters returned to baseline values as found in untreated C3H/HeJ mice (Fig. 6C). While the number of activated astrocytes remained increased on Day25, the number of SWDs that had started to recover on Day7 unexpectedly dropped again on Day25. The increase in the percentage of wakefulness on Day25 may at least partially explain this finding. In addition, different pro-inflammatory cytokines modulated I_h current properties ($V_{0.5}$, current density) and rhythmic burst activity in an opposing manner.

These findings highlight that the generation of SWDs requires an intact TC system and HCN channel activity in VB TC neurons. The degree of myelination in different parts of the TC system and the action of inflammatory cytokines constitute a logical matrix of parameters underlying the occurrence of epileptic activity in MS models.

General Demyelination and Epileptic Activity

In previous studies, prolonged chronic cuprizone treatment (9–12 weeks) in C5BL/6J mice induced epileptic seizures in the hippocampus that were associated with extensive demyelination, axonal damage, neuronal loss, and widespread gliosis (Hoffmann et al. 2008; Lapato et al. 2017). In our study, we used an established mouse model of absence epilepsy, a condition characterized by increased excitation. Unexpectedly, acute demyelination caused by 5 weeks cuprizone treatment in C3H/HeJ mice was not associated with an increased occurrence of epileptic activity. Instead, cuprizone-treated C3H/HeJ mice demonstrated a significant decrease in the number of SWDs on Day1. Thereafter, the occurrence of SWDs increased again on Day7 but dropped on Day25 (Fig. 1). As discussed in the following paragraphs, several factors may influence this complex time course.

Fundamentally, demyelination leads to slowed conduction velocities and delayed propagation of activity between different neuronal populations, thereby altering network dynamics (Crawford et al. 2009; Cerina et al. 2018). In WAG/Rij, rats the paroxysmal oscillation within the TC system are based on large-scale synchronization and fast intracortical spread of seizure activity

(Meeren et al. 2002). Graph theory and neural dynamics modeling of the human brain network emphasize the importance of the space–time structure of coupling defined by the anatomical connectivity and the time delays in the emergence of global synchronization during the generation of SWDs (Yan and Li 2013). Demyelinated axons may not be able to meet these requirements, thereby resulting in decreased SWD generation during early remyelination. In addition, changes in network organization during seizures like the segregation of cortical regions from the remaining brain may play a role (Wachsmuth et al. 2021). At later stages, poor properties of the regenerated myelin may play a role. It has been shown that remyelinated sheaths are thinner, less tight and differentially distributed along the axons (Stidworthy et al. 2003; Crawford et al. 2009; Zendedel et al. 2013; Praet et al. 2014; Brousse et al. 2016). Furthermore, HCN channels have been shown to play an important role in the generation of epileptic activity in the TC system. In rodent absence epilepsy models (GAERS and WAG/Rij rats), the occurrence of SWDs is correlated with increased I_h amplitudes in TC neurons from different thalamic nuclei (Kanyshkova et al. 2012; Cain et al. 2015) and pharmacological block of HCN channels with ZD7288 in the VB of freely moving GAERS rats can abolish absence seizures (Dyhrfjeld-Johnsen et al. 2009). Therefore, the temporal pattern of I_h availability at the early time points (strong reduction of the current on Day1, initial increase in current on Day7) is in accordance with the numbers of SWDs. On Day25, however, there is a divergence from this scheme, indicating the influence of additional factors.

With regard to this, cortical influences should be considered, since a hyperexcitable focus in S1 has been suggested as the initial trigger zone for SWD generation (Meeren et al. 2002). In WAG/Rij rats, the reduction of I_h in neocortical neurons of S1, which results in increased membrane excitability, is associated with the generation of absence seizures. Indeed, in cuprizone-treated C57BL/6J mice, we observed strongly reduced cortical excitability on Days 1 and 25 with an interlude of transient hyperexcitability on Day7 (Cerina et al. 2018). This pattern of changed excitability was accompanied by permanent alterations in the spread of activity in the primary auditory cortex (A1). Furthermore, long-term potentiation and the tonotopic organization in A1, two phenomena requiring temporally fine adjusted synchronized activity were reduced and lost at Day25, respectively (Ghaffarian et al. 2016; Cerina et al. 2017, 2018). Thus, proper maintenance of epileptic activity requires a substantial level of I_h in both thalamus and cortex with I_h availability determining the level of network synchronization and therefore seizure prevalence. Different cytokines, such as IFN-α and IFN-β, may also affect thalamic and cortical HCN channels (Stadler et al. 2014), which further emphasize the relationship between the demyelination-induced inflammation and the epileptic seizures. However, the contribution of cortical I_h to seizure activity after the process of acute demyelination has to be thoroughly investigated in the future. In addition, altered levels of I_h and HCN channel expression represent just one possible mechanism that influences the number of SWDs and cannot solely explain the deviations seen in the SWDs characteristic during different stages of remyelination.

In a model of focal demyelination, lysolecithin-induced lesions in A1 strongly reduced bursting in the ventral part of the medial geniculate nucleus at 28 days after injection, thereby demonstrating the strong influence of cortical mechanisms on thalamic activity modes (Narayanan et al. 2018). These findings indicate that demyelination followed by functionally inadequate remyelination may decrease the level of synchronization of neuronal activity and cellular excitability in the CNS, thereby restraining the cortical pacemaker function and spread of activity in the TC network in absence epilepsy. Demyelination-induced changes in ion channel function may contribute to this disordered network. In the present study, acute demyelination decreased HCN channel activity in TC neurons, limited rhythmic oscillations in the thalamus and SWD generation in the TC system. The distribution and expression of other ion channels, like Na_V 1.6, K_V 1.3, and K_V 7.3, may also be changed by demyelinating events (Rus et al. 2005; Hamada et al. 2016; Bozic et al. 2018). Computer modeling indicates that an increase in K_V 7 channel function limits rhythmic activity in the TC network model. This points to the interesting possibility that specific blockers of HCN4 channels, the major thalamic isoform, and specific activators of K_V7 channels may control epileptic activity in the TC system (Eskioglou et al. 2018; Romanelli et al. 2019; Kharouf, Phillips, et al. 2020; Kharouf, Pinares-Garcia, et al. 2020).

Additional cellular and network changes may trigger or modulate SWD activity in C3H/HeJ mice following demyelination. In this respect, alterations in (1) AMPA-receptor dependent synaptic activity, (2) in limbic-TC interactions, (3) in the function of GABAergic interneurons and (4) in the focal onset zone, as well as (5) differences in the speed of remyelination in different white matter tracts may play a role.

1) The major determinant of SWDs in C3H/HeJ mice is a mutation of the AMPA receptor subunit *Gria4*, which is predominantly present in TRN neurons and thereby inducing abnormal synaptic activity in the thalamus and contributing to the occurrence of absence seizures (Beyer et al. 2008; Ellens et al. 2009). Future studies have to address altered AMPA receptor-dependent synaptic activity following cuprizone treatment.
2) Previous studies have shown an effect of increased excitability in the limbic system on SWD generation in the TC system of rats (Aker et al. 2006; Çarçak et al. 2008). However, hippocampal recordings in

C3H/HeJ mice revealed no difference in theta activity during and between SWDs thereby indicating no major contribution of this brain structure to SWD generation in this model (Frankel 2005). Future studies have to investigate the presence of subclinical seizures in limbic structures that might contribute to the occurrence of SWDs in C3H/HeJ mice.

3) PV^+ interneurons are an important cellular element influencing neuronal network excitability in different brain regions (Bartholome et al. 2020) and the occurrence of absence seizures in rats (Arkan et al. 2019). There seem to be a selective vulnerability of inhibitory networks in motor cortex in MS patients and following focal cortical demyelination (Zoupi et al. 2021). In addition, prolonged (9–12 weeks) cuprizone treatment induces the loss of PV^+ interneurons in the hippocampal CA1 subregion (Lapato et al. 2017). However, shorter (5 weeks) cuprizone-induced hippocampal demyelination was not associated with an overall loss of neurons in dentate gyrus (Zhu et al. 2021). Here, we performed NeuN staining in the hippocampal CA1 region, neocortex and thalamus and assessed the number of PV^+ neurons in TRN. No differences in the number of $NeuN^+$ cells were found between C3H/HeJ controls and mice on Day1 in neocortex, CA1 and different compartments of the TRN. In addition, no differences in PV^+ neurons were found in TRN as an important pacemaker for slow TC oscillations. These findings demonstrate no changes in the overall number of neurons thereby indicating lack of major neurodegenerative processes in the present cuprizone model. Importantly TRN PV^+ cells that are preferentially rhythmogenic and can disrupt TC seizures (Clemente-Perez et al. 2017) are unchanged. Therefore, we conclude that changes in the composition of TRN neurons do not contribute to the changes in the occurrence of SWDs in the present cuprizone model. Since different rat models of absence epilepsy show divergent alterations of PV^+ interneurons in specific cortical regions (Papp et al. 2018), future studies have to unravel changes in the function of GABAergic neurons in different brain regions in the cuprizone model.
4) Multiple lines of evidence have suggested that SWDs are not primarily generalized despite its definition, but rather involve particular neuronal networks with focal cortical onset in rats (Meeren et al. 2002, 2005; Lee et al. 2019). Spikes may originate around the cortical somatosensory areas and the thalamus provides a resonant circuitry to amplify and sustain the discharges. Indeed, a mouse model with a juvenile myoclonic epilepsy mutation in a $GABA_A$ receptor $\alpha 1$ subunit exhibited both absence and myoclonic generalized seizures that were first detected in S1 and propagated to M1 (Ding and Gallagher 2016). However, different cortical networks can be involved in the generation of SWDs across different pharmacological (gamma-hydroxybutyric acid) and genetic (phospholipase beta4 knock-out) mouse models (Lee et al. 2019). Future studies have to identify possible alteration in the epileptic cortical initiation zone or segregation of the cortex from subcortical areas in the course of seizures following demyelination (Wachsmuth et al. 2021).
5) Regional heterogeneity of cuprizone-induced demyelination has been observed (Zhan et al. 2020). While demyelination was severe within the corpus callosum, loss of myelin staining intensity was by far less severe in the white matter tract fornix. Depending on the position within the brain (rostral, occipital) the medial or lateral parts of the corpus callosum are inversely affected. Also in the present study, demyelination of the IC was not complete. In addition to the expected demyelination in the corpus callosum, the cortex of C57BL/6 mice was completely demyelinated after 6 weeks of cuprizone feeding (Skripuletz et al. 2008). Following a prolonged period of cuprizone feeding (12 weeks), cortical remyelination was significantly delayed. Moreover, in BALB/cJ mice cortical demyelination was only partial. These findings demonstrates that different and even neighboring white matter tracts as well as gray matter areas display distinct and strain-specific vulnerability to cuprizone-induced demyelination that may contribute to changes in SWD generation found in the present study. Future studies have to elucidate the fiber tract-specific demyelination and remyelination pattern in C3H/HeJ mice.

Demyelination Reduced HCN Channels Activity

In the present study, I_h current amplitudes were found to be significantly reduced in cuprizone-treated C3H/HeJ mice on Days 1 and 7 in comparison with C3H/HeJ control. On Day25, I_h parameters became similar to C3H/HeJ control mice values. In line with previous studies, during which reduction of I_h occurred, the myelin-induced decrease in I_h resulted in a hyperpolarizing shift in the RMP of TC neurons (Dyhrfjeld-Johnsen et al. 2009). It also caused a significant hyperpolarization shift in the voltage-dependent activation of I_h and slowed activation kinetics of HCN channels on Days 1 and 7. While the latter findings would be in line with decreased cyclic nucleotide-dependent modulation of I_h (Datunashvili et al. 2018), we hypothesize that demyelination may cause changes in the expression or localization of HCN channels. In this respect, HCN channel interacting proteins may be relevant. The auxiliary subunit TRIP8b is important for the membrane surface expression and subcellular localization of HCN channel along the axonal and somatodendritic axis (Wilkars et al. 2012). Since TRIP8b is downregulated under neuroinflammatory conditions in the hippocampus, it may be involved

in the observed effects (Frigerio et al. 2018). Indeed the loss of TRIP8b results in a strong reduction of I_h current density in TC neurons (Zobeiri et al. 2018). In the present study, the decreased HCN channel expression was associated with deceased expression of pS237-TRIP8b, which is sufficient to alter HCN channel function in the hippocampus (Foote et al. 2019). The idea of decreased phosphorylation is in line with the decreased staining obtained by the neurofilament antibody used here that reacts against extensively phosphorylated axonal epitopes on neurofilaments M and H.

General Demyelination and Increased Slow TC Activity

In addition to reduction in seizure activity after strong general demyelination, analysis of interictal cortical LFP recordings in cuprizone-treated C3H/HeJ mice on Days 1, 7, and 25 revealed a general increase in slow TC oscillations in the θ frequency range. Increased low-frequency rhythmicity (δ and θ) in the TC system during the wake state is a characteristic feature of TCD, and has been previously reported in a number of neurological and psychiatric disorders (Llinás et al. 1999), as well as in patients with MS (Leocani et al. 2000; Leocani and Comi 2000; Krupina et al. 2020). Quantitative EEG studies of patients with MS show higher θ but also δ band PSD and a lower alpha band, which is particularly related to cognitive dysfunction. Clearly, the axonal damage and widespread gray matter pathology in MS patients is responsible for changes in cortico-cortical and TC connectivity and consequently alteration in TC rhythms. The observed increase in interictal θ activity induced by acute demyelination is consistent with the results of our previous studies in which reduction of I_h in thalamic relay neurons caused a significant increase in δ or θ frequency oscillations (Datunashvili et al. 2018; Zobeiri et al. 2018). Other studies also indicate a strong association between downregulation of I_h or HCN channel deletion in the cortex and increased δ and θ frequency oscillations during the wake state and sleep (Krupina et al. 2020). While cortical I_h is essential for generation and maintenance of rhythmic subthreshold membrane potential oscillations and θ resonance activity, thalamic I_h is involved in the generation of rhythmic burst activity and slow frequency oscillations that are mostly observed during sleep, but also during anesthesia and under some pathophysiological conditions such as epilepsy (Biel et al. 2009; He et al. 2014). In addition to I_h, θ resonance in cortical neurons is shaped by the close interplay of other types of ionic conductance such as the M-current (I_M) and the persistent Na^+ current, I_{NaP} (Dickson et al. 2000; Hu et al. 2002). Whether changes in the slow frequency oscillations during different stages of remyelination are caused by interaction between I_h and I_M or are solely dependent on dysregulation of HCN channels needs further investigation.

Modulatory Effects of Cytokines on Network Oscillatory Activity

In our study IL-1β increased the intrathalamic burst activity in C3H/HeJ controls and on Day25 but there was no significant effect of IL-1β in on Days 1 and 7. The reason for this is not clear. However, based on the reciprocal interaction of TC and TRN neurons in this type of network activity, effects on TRN neurons and synaptic interactions that were not investigated here may play a role. Furthermore, a decrease in burst activity induced by IFN-α was observed for all experimental conditions. On Days 1 and 7, TC network was shifted toward decreased activity and the application of IFN-α caused further membrane hyperpolarization and reduction in burst activity. Thus, regardless of the degree of myelination, IFN-α was able to significantly reduce burst activity, indicating that additional mechanisms may regulate the IFN-α effect on HCN channels and rhythmic burst activity. It should be noted here that microglia activation in the cuprizone model demonstrates different phases (Plastini et al. 2020). Specifically, during demyelination, microglia produce cytokines that support inflammation and demyelination, including IFN-α. Later, microglia are involved in reparative remyelination and reveal a different cytokine repertoire, including IL-1β. Thus, the effects of these cytokines on I_h are in line with the early reduction and later reconstitution of the pacemaker current found in the present study.

Mathematical Modeling of the Role of HCN Channels in Oscillatory Bursting

By computing experimentally obtained parameters in a simplified intrathalamic network model, we proved that changes in I_h properties might largely contribute to the observed changes in intrathalamic oscillatory activity in horizontal slices. In addition, we observed a complex dependency of the number bursts on the magnitude of two I_h parameters that determine the availability of HCN channels, namely $V_{0.5}$ and current density. By including former modeling results into account (Datunashvili et al. 2018; Zobeiri et al. 2018), we found that there is a rather small range of $V_{0.5}$ and current density values in which HCN channel function optimally to sustain slow rhythmic burst activity. Deviations from this parameter space leads to a decrease in oscillatory burst activity.

Demyelination Influenced the Cellular and Electrophysiological Parameters in the TC System of C3H/HeJ Control Mice Compared to C3H/HeJ Mice Treated with Cuprizone

Cuprizone treatment modulated I_h parameters (current density, $V_{0.5}$), thalamic bursting, the occurrence of SWDs, the degree of myelination, the numbers of oligodendrocytes, and the activation of astrocytes and microglia. The summarizing plots (Fig. 6) of these parameters against the different experimental conditions revealed that all of them deviated from baseline values on Day1 and approached baseline values again on Day25. Numbers

of activated astrocytes and microglia were increased on Day1 whereas current density, $V_{0.5}$, burst activity, SWDs, degree of myelination and numbers of oligodendrocytes were decreased showing that the time point of maximum demyelination was associated with astrogliosis, signs of inflammation, low HCN channel availability and a strong decrease in TC network activity. Together with the finding that IFN-α and IL-1β have opposite effects on I_h and TC network oscillations, our study provides evidence that in MS models and potentially MS patients the combinatory effects of demyelination, inflammatory cytokines, and neurodegeneration determine the degree of synchronous neuronal activity and the occurrence of epileptic seizures. Demyelinated neuronal networks sustain epileptic activity to a lesser degree and may no longer support seizures when damage accumulates.

Supplementary Material

Supplementary material can be found at *Cerebral Cortex* online.

Funding

Deutsche Forschungsgemeinschaft (grant numbers RTG 2515-1 to T.B. and S.G.M., SFB-TR 128-B06 to T.B. and S.G.M., SFB-TR 128-B07 to T.K., BU1019/16-1 to T.B.).

Notes

The authors thank Claudia Kemming, Svetlana Kiesling, Elke Naß, and Frank Kurth for excellent technical assistance and Dr Dilip Verma for insightful scientific discussion of the results. *Conflict of Interest*: None declared.

References

Aker RG, Yananli HR, Gurbanova AA, Özkaynakçi AE, Ateş N, van Luijtelaar G, Onat FY. 2006. Amygdala kindling in the WAG/Rij rat model of absence epilepsy. *Epilepsia*. 47: 33–40.

Araújo SES, Mendonça HR, Wheeler NA, Campello-Costa P, Jacobs KM, Gomes FCA, Fox MA, Fuss B. 2017. Inflammatory demyelination alters subcortical visual circuits. *J Neuroinflammation*. 14:162.

Arkan S, Kasap M, Akman Ö, Akpınar G, Ateş N, Karson A. 2019. The lower expression of parvalbumin in the primary somatosensory cortex of WAG/Rij rats may facilitate the occurrence of absence seizures. *Neurosci Lett*. 709:134299.

Bartholome O, de la Brassinne BO, Neirinckx V, Rogister B. 2020. A composite sketch of fast-spiking parvalbumin-positive neurons. *Cereb Cortex Commun*. 1:1–15.

Beyer B, Deleuze C, Letts VA, Mahaffey CL, Boumil RM, Lew TA, Huguenard JR, Frankel WN. 2008. Absence seizures in C3H/HeJ and knockout mice caused by mutation of the AMPA receptor subunit Gria4. *Hum Mol Genet*. 17:1738–1749.

Biel M, Wahl-Schott C, Michalakis S, Zong X. 2009. Hyperpolarization-activated cation channels: from genes to function. *Physiol Rev*. 89: 847–885.

Bittner S, Ruck T, Wiendl H, Grauer OM, Meuth SG. 2017. Targeting B cells in relapsing-remitting multiple sclerosis: from pathophysiology to optimal clinical management. *Ther Adv Neurol Disord*. 10: 51–66.

Bozic I, Tesovic K, Laketa D, Adzic M, Jakovljevic M, Bjelobaba I, Savic D, Nedeljkovic N, Pekovic S, Lavrnja I. 2018. Voltage gated potassium channel Kv1.3 is upregulated on activated astrocytes in experimental autoimmune encephalomyelitis. *Neurochem Res*. 43:1020–1034.

Brousse B, Magalon K, Durbec P, Cayre M. 2016. Region and dynamic specificities of adult neural stem cells and oligodendrocyte precursors in myelin regeneration in the mouse brain. *Biol Open*. 5: 204–204.

Budde T, Caputi L, Kanyshkova T, Staak R, Abrahamczik C, Munsch T, Pape H. 2005. Impaired regulation of thalamic pacemaker channels through an Imbalance of subunit expression in absence epilepsy. *J Neurosci*. 25:9871–9882.

Burman J, Zelano J. 2017. Epilepsy in multiple sclerosis: a nationwide population-based register study. *Neurology*. 89:2462–2468.

Cain SM, Tyson JR, Jones KL, Snutch TP. 2015. Thalamocortical neurons display suppressed burst-firing due to an enhanced Ih current in a genetic model of absence epilepsy. *Pflügers Arch - Eur J Physiol*. 467:1367–1382.

Calabrese M, De Stefano N, Atzori M, Bernardi V, Mattisi I, Barachino L, Rinaldi L, Morra A, McAuliffe MMJ, Perini P, et al. 2008. Extensive cortical inflammation is associated with epilepsy in multiple sclerosis. *J Neurol*. 255:581–586.

Cano A, Fonseca E, Ettcheto M, Sánchez-López E, de Rojas I, Alonso-Lana S, Morató X, Souto EB, Toledo M, Boada M, et al. 2021. Epilepsy in neurodegenerative diseases: related drugs and molecular pathways. *Pharmaceuticals (Basel)*. 14:1057.

Çarçak N, Aker RG, Özdemir O, Demiralp T, Onat FY. 2008. The relationship between age-related development of spike-and-wave discharges and the resistance to amygdaloid kindling in rats with genetic absence epilepsy. *Neurobiol Dis*. 32:355–363.

Cerina M, Narayanan V, Göbel K, Bittner S, Ruck T, Meuth P, Herrmann AM, Stangel M, Gudi V, Skripuletz T, et al. 2017. The quality of cortical network function recovery depends on localization and degree of axonal demyelination. *Brain Behav Immun*. 59:103–117.

Cerina M, Narayanan V, Delank A, Meuth P, Graebenitz S, Göbel K, Herrmann AM, Albrecht S, Daldrup T, Seidenbecher T, et al. 2018. Protective potential of dimethyl fumarate in a mouse model of thalamocortical demyelination. *Brain Struct Funct*. 223:3091–3106.

Cerina M, Muthuraman M, Gallus M, Koirala N, Dik A, Wachsmuth L, Hundehege P, Schiffler P, Tenberge JG, Fleischer V, et al. 2020. Myelination- and immune-mediated MR-based brain network correlates. *J Neuroinflammation*. 17:1–16.

Clemente-Perez A, Makinson SR, Higashikubo B, Brovarney S, Cho FS, Urry A, Holden SS, Wimer M, Dávid C, Fenno LE, et al. 2017. Distinct thalamic reticular cell types differentially modulate normal and pathological cortical rhythms. *Cell Rep*. 19:2130–2142.

Coenen AML, Drinkenburg WHIM, Peeters BWMM, Vossen JMH, van Luijtelaar ELJM. 1991. Absence epilepsy and the level of vigilance in rats of the WAG/Rij strain. *Neurosci Biobehav Rev*. 15:259–263.

Colombo E, Farina C. 2016. Astrocytes: key regulators of neuroinflammation. *Trends Immunol*. 37:608–620.

Crawford DK, Mangiardi M, Xia X, López-Valdés HE, Tiwari-Woodruff SK. 2009. Functional recovery of callosal axons following demyelination: a critical window. *Neuroscience*. 164:1407–1421.

Crunelli V, David F, Leresche N, Lambert RC. 2014. Role for T-type Ca^{2+}channels in sleep waves. *Pflugers Arch Eur J Physiol*. 466: 735–745.

Crunelli V, Lorincz ML, McCafferty C, Lambert RC, Leresche N, Di Giovanni G, David F. 2020. Clinical and experimental insight into pathophysiology, comorbidity and therapy of absence seizures. *Brain*. 143:2341–2368.

Datunashvili M, Chaudhary R, Zobeiri M, Lüttjohann A, Mergia E, Baumann A, Balfanz S, Budde B, van Luijtelaar G, Pape H-C, et al. 2018. Modulation of hyperpolarization-activated inward current and thalamic activity modes by different cyclic nucleotides. *Front Cell Neurosci*. 12:369.

Deppe M, Krämer J, Tenberge JG, Marinell J, Schwindt W, Deppe K, Groppa S, Wiendl H, Meuth SG. 2016. Early silent microstructural degeneration and atrophy of the thalamocortical network in multiple sclerosis. *Hum Brain Mapp*. 37:1866–1879.

Destexhe A, Bal T, McCormick DA, Sejnowski TJ. 1996. Ionic mechanisms underlying synchronized oscillations and propagating waves in a model of ferret thalamic slices. *J Neurophysiol*. 76: 2049–2070.

Destexhe A, Contreras D, Steriade M. 1998. Mechanisms underlying the synchronizing action of corticothalamic feedback through inhibition of thalamic relay cells. *J Neurophysiol*. 79:999–1016.

Dickson CT, Magistretti J, Shalinsky MH, Fransén E, Hasselmo ME, Alonso A. 2000. Properties and role of I(h) in the pacing of subthreshold oscillations in entorhinal cortex layer II neurons. *J Neurophysiol*. 83:2562–2579.

Ding L, Gallagher MJ. 2016. Dynamics of sensorimotor cortex activation during absence and myoclonic seizures in a mouse model of juvenile myoclonic epilepsy. *Epilepsia*. 57:1568–1580.

Durmus H, Kurtuncu M, Tuzun E, Pehlivan M, Akman-Demir G, Yapıcı Z, Eraksoy M. 2013. Comparative clinical characteristics of early- and adult-onset multiple sclerosis patients with seizures. *Acta Neurol Belg*. 113:421–426.

Dyhrfjeld-Johnsen J, Morgan RJ, Soltesz I. 2009. Double trouble? Potential for hyperexcitability following both channelopathic up- and downregulation of Ih in epilepsy. *Front Neurosci*. 3:25–33.

Ehling P, Kanyshkova T, Baumann A, Landgraf P, Meuth SG, Pape HC, Budde T. 2012. Adenylyl cyclases: expression in the developing rat thalamus and their role in absence epilepsy. *J Mol Neurosci*. 48: 45–52.

Ellens DJ, Hong E, Giblin K, Singleton MJ, Bashyal C, Englot DJ, Mishra AM, Blumenfeld H. 2009. Development of spike-wave seizures in C3H/HeJ mice. *Epilepsy Res*. 85:53–59.

Eskioglou E, Perrenoud MP, Ryvlin P, Novy J. 2018. Novel treatment and new drugs in epilepsy treatment. *Curr Pharm Des*. 23: 6389–6398.

Filippi M, Bar-Or A, Piehl F, Preziosa P, Solari A, Vukusic S, Rocca MA. 2018. Multiple sclerosis. *Nat Rev Dis Prim*. 4:1–27.

Foote KM, Lyman KA, Han Y, Michailidis IE, Heuermann RJ, Mandikian D, Trimmer JS, Swanson GT, Chetkovich DM. 2019. Phosphorylation of the HCN channel auxiliary subunit TRIP8b is altered in an animal model of temporal lobe epilepsy and modulates channel function. *J Biol Chem*. 294:15743–15758.

Frankel WN. 2005. Development of a new genetic model for absence epilepsy: spike-wave seizures in C3H/He and backcross mice. *J Neurosci*. 25:3452–3458.

Frigerio F, Flynn C, Han Y, Lyman K, Lugo JN, Ravizza T, Ghestem A, Pitsch J, Becker A, Anderson AE, et al. 2018. Neuroinflammation alters integrative properties of rat hippocampal pyramidal cells. *Mol Neurobiol*. 55:7500–7511.

Ghaffarian N, Mesgari M, Cerina M, Göbel K, Budde T, Speckmann EJ, Meuth SG, Gorji A. 2016. Thalamocortical-auditory network alterations following cuprizone-induced demyelination. *J Neuroinflammation*. 13:1–11.

Graeber MB, Li W, Rodriguez ML. 2011. Role of microglia in CNS inflammation. *FEBS Lett*. 585:3798–3805.

Hamada MS, Kole MHP. 2015. Myelin loss and axonal ion channel adaptations associated with gray matter neuronal hyperexcitability. *J Neurosci*. 35:7272–7286.

Hamada MS, de Vries SI, Kole MHP, Brette R, Goethals S. 2016. Covariation of axon initial segment location and dendritic tree normalizes the somatic action potential. *Proc Natl Acad Sci*. 113: 14841–14846.

Han Y, Lyman KA, Foote KM, Chetkovich DM. 2020. The structure and function of TRIP8b, an auxiliary subunit of hyperpolarization-activated cyclic-nucleotide gated channels. *Channels*. 14:110.

He C, Chen F, Li B, Hu Z. 2014. Neurophysiology of HCN channels: from cellular functions to multiple regulations. *Prog Neurobiol*. 112:1–23.

Heuermann RJ, Jaramillo TC, Ying S-W, Suter BA, Lyman KA, Han Y, Lewis AS, Hampton TG, Shepherd GMG, Goldstein PA, et al. 2016. Reduction of thalamic and cortical Ih by deletion of TRIP8b produces a mouse model of human absence epilepsy. *Neurobiol Dis*. 85:81–92.

Hines ML, Carnevale NT. 2001. NEURON: a tool for neuroscientists. *Neuroscientist*. 7:123–135.

Hiremath MM, Saito Y, Knapp GW, Ting JPY, Suzuki K, Matsushima GK. 1998. Microglial/macrophage accumulation during cuprizone-induced demyelination in C57BL/6 mice. *J Neuroimmunol*. 92:38–49.

Hoffmann K, Lindner M, Gröticke I, Stangel M, Löscher W. 2008. Epileptic seizures and hippocampal damage after cuprizone-induced demyelination in C57BL/6 mice. *Exp Neurol*. 210: 308–321.

Hu H, Vervaeke K, Storm JF. 2002. Two forms of electrical resonance at theta frequencies, generated by M-current, h-current and persistent Na+ current in rat hippocampal pyramidal cells. *J Physiol*. 545:783–805.

Huber R, Deboer T, Tobler I. 2000. Topography of EEG dynamics after sleep deprivation in mice. *J Neurophysiol*. 84:1888–1893.

Huguenard JR, Prince D. 1994. Intrathalamic rhythmicity studied in vitro: nominal T-current modulation causes robust antioscillatory effects. *J Neurosci*. 14:5485–5502.

Kanyshkova T, Pawlowski M, Meuth P, Dube C, Bender RA, Brewster AL, Baumann A, Baram TZ, Pape H-C, Budde T. 2009. Postnatal expression pattern of HCN channel isoforms in thalamic neurons: relationship to maturation of thalamocortical oscillations. *J Neurosci*. 29:8847–8857.

Kanyshkova T, Meuth P, Bista P, Liu Z, Ehling P, Caputi L, Doengi M, Chetkovich DM, Pape HC, Budde T. 2012. Differential regulation of HCN channel isoform expression in thalamic neurons of epileptic and non-epileptic rat strains. *Neurobiol Dis*. 45:450–461.

Kavčič A, Hofmann WE. 2017. Unprovoked seizures in multiple sclerosis: why are they rare? *Brain Behav*. 7:e00726.

Kelley BJ, Rodriguez M. 2009. Seizures in patients with multiple sclerosis: epidemiology, pathophysiology and management. *CNS Drugs*. 23:805–815.

Kharouf Q, Phillips AM, Bleakley LE, Morrisroe E, Oyrer J, Jia L, Ludwig A, Jin L, Nicolazzo JA, Cerbai E, et al. 2020. The hyperpolarization-activated cyclic nucleotide-gated 4 channel as a potential anti-seizure drug target. *Br J Pharmacol*. 177:3712–3729.

Kharouf Q, Pinares-Garcia P, Romanelli MN, Reid CA. 2020. Testing broad-spectrum and isoform-preferring HCN channel blockers for anticonvulsant properties in mice. *Epilepsy Res*. 168:106484.

Kipp M, van der Valk P, Amor S. 2012. Pathology of multiple sclerosis. *CNS Neurol Disord - Drug Targets*. 11:506–517.

Kipp M, Wagenknecht N, Beyer C, Samer S, Wuerfel J, Nikoubashman O. 2015. Thalamus pathology in multiple sclerosis: from biology to clinical application. *Cell Mol Life Sci*. 72:1127–1147.

Krupina NA, Churyukanov MV, Kukushkin ML, Yakhno NN. 2020. Central neuropathic pain and profiles of quantitative electroencephalography in multiple sclerosis patients. *Front Neurol*. 10:1380.

Langenbruch L, Krämer J, Güler S, Möddel G, Geßner S, Melzer N, Elger CE, Wiendl H, Budde T, Meuth SG, et al. 2019. Seizures and epilepsy in multiple sclerosis: epidemiology and prognosis in a large tertiary referral center. *J Neurol*. 266:1789–1795.

Lapato AS, Szu JI, Hasselmann JPC, Khalaj AJ, Binder DK, Tiwari-Woodruff SK. 2017. Chronic demyelination-induced seizures. *Neuroscience*. 346:409–422.

Lee S, Hwang E, Lee M, Choi JH. 2019. Distinct topographical patterns of spike-wave discharge in transgenic and pharmacologically induced absence seizure models. *Exp Neurobiol*. 28:474.

Leocani L, Comi G. 2000. Neurophysiological investigations in multiple sclerosis. *Curr Opin Neurol*. 13:255–261.

Leocani L, Locatelli T, Martinelli V, Rovaris M, Falautano M, Filippi M, Magnani G, Comi G. 2000. Electroencephalographic coherence analysis in multiple sclerosis: correlation with clinical, neuropsychological, and MRI findings. *J Neurol Neurosurg Psychiatry*. 69: 192–198.

Leresche N, Lambert RC, Errington AC, Crunelli V. 2012. From sleep spindles of natural sleep to spike and wave discharges of typical absence seizures: is the hypothesis still valid? *Pflugers Arch Eur J Physiol*. 463:201–212.

Llinás RR, Ribary U, Jeanmonod D, Kronberg E, Mitra PP. 1999. Thalamocortical dysrhythmia: a neurological and neuropsychiatric syndrome characterized by magnetoencephalography. *Proc Natl Acad Sci U S A*. 96:15222–15227.

Ludwig A, Budde T, Stieber J, Moosmang S, Wahl C, Holthoff K, Langebartels A, Wotjak C, Munsch T, Zong X, et al. 2003. Absence epilepsy and sinus dysrhythmia in mice lacking the pacemaker channel HCN2. *EMBO J*. 22:216–224.

Meeren HKM, Pijn JPM, Van Luijtelaar ELJM, Coenen AML, Lopes da Silva FH. 2002. Cortical focus drives widespread corticothalamic networks during spontaneous absence seizures in rats. *J Neurosci*. 22:1480–1495.

Meeren H, van Luijtelaar G, Lopes da Silva F, Coenen A. 2005. Evolving concepts on the pathophysiology of absence seizures: the cortical focus theory. *Arch Neurol*. 62:371–376.

Meuth P, Meuth SG, Jacobi D, Broicher T, Pape H, Budde T. 2005. Get the rhythm: modeling neuronal activity. *J Undergr Neurosci Educ*. 4:1–11.

Mirmosayyeb O, Shaygannejad V, Nehzat N, Mohammadi A, Ghajarzadeh M. 2021. Prevalence of seizure/epilepsy in patients with multiple sclerosis: a systematic review and meta-analysis. *Int J Prev Med*. 12:14.

Narayanan V, Cerina M, Göbel K, Meuth P, Herrmann AM, Fernandez-Orth J, Stangel M, Gudi V, Skripuletz T, Daldrup T, et al. 2018. Impairment of frequency-specific responses associated with altered electrical activity patterns in auditory thalamus following focal and general demyelination. *Exp Neurol*. 309:54–66.

Neuß F, von Podewils F, Wang ZI, Süße M, Zettl UK, Grothe M. 2020. Epileptic seizures in multiple sclerosis: prevalence, competing causes and diagnostic accuracy. *J Neurol*. 268:1721–1727.

Pack A. 2018. Is there a relationship between multiple sclerosis and epilepsy? If so what does it tell us about epileptogenesis? *Epilepsy Curr*. 18:95–96.

Papp P, Kovács Z, Szocsics P, Juhász G, Maglóczky Z. 2018. Alterations in hippocampal and cortical densities of functionally different interneurons in rat models of absence epilepsy. *Epilepsy Res*. 145: 40–50.

Peferoen L, Kipp M, van der Valk P, van Noort JM, Amor S. 2014. Oligodendrocyte-microglia cross-talk in the central nervous system. *Immunology*. 141:302–313.

Pinault D, O'Brien T. 2005. Cellular and network mechanisms of genetically-determined absence seizures. *Thalamus Relat Syst*. 3: 181–203.

Plastini MJ, Desu HL, Brambilla R. 2020. Dynamic responses of microglia in animal models of multiple sclerosis. *Front Cell Neurosci*. 14:269.

Poser CM, Brinar VV. 2003. Epilepsy and multiple sclerosis. *Epilepsy Behav*. 4:6–12.

Praet J, Guglielmetti C, Berneman Z, Van der Linden A, Ponsaerts P. 2014. Cellular and molecular neuropathology of the cuprizone mouse model: clinical relevance for multiple sclerosis. *Neurosci Biobehav Rev*. 47:485–505.

Romanelli MN, Del LM, Guandalini L, Zobeiri M, Gyökeres A, Árpádffy-Lovas T, Koncz I, Sartiani L, Bartolucci G, Dei S, et al. 2019. EC18 as a tool to understand the role of HCN4 channels in mediating hyperpolarization-activated current in tissues. *ACS Med Chem Lett*. 10:584–589.

Ruck T, Bittner S, Gross CC, Breuer J, Albrecht S, Korr S, Göbel K, Pankratz S, Henschel CM, Schwab N, et al. 2013. CD4+NKG2D+ T cells exhibit enhanced migratory and encephalitogenic properties in neuroinflammation. *PLoS One*. 8:e81455.

Rus H, Pardo CA, Hu L, Darrah E, Cudrici C, Niculescu T, Niculescu F, Mullen KM, Allie R, Guo L, et al. 2005. The voltage-gated potassium channel Kv1.3 is highly expressed on inflammatory infiltrates in multiple sclerosis brain. *Proc Natl Acad Sci*. 102: 11094–11099.

Samios VN, Inoue T. 2014. Interleukin-1β and interleukin-6 affect electrophysiological properties of thalamic relay cells. *Neurosci Res*. 87:16–25.

Skripuletz T, Lindner M, Kotsiari A, Garde N, Fokuhl J, Linsmeier F, Trebst C, Stangel M. 2008. Cortical demyelination is prominent in the murine cuprizone model and is strain-dependent. *Am J Pathol*. 172:1053.

Skripuletz T, Gudi V, Hackstette D, Stangel M. 2011. De- and remyelination in the CNS white and grey matter induced by cuprizone: The old, the new, and the unexpected. *Histol Histopathol*. 26: 1585–1597.

Stadler K, Bierwirth C, Stoenica L, Battefeld A, Reetz O, Mix E, Schuchmann S, Velmans T, Rosenberger K, Bräuer AU, et al. 2014. Elevation in type i interferons inhibits HCN1 and slows cortical neuronal oscillations. *Cereb Cortex*. 24:199–210.

Stidworthy MF, Genoud S, Suter U, Mantei N, Franklin RJ. 2003. Quantifying the early stages of remyelination following cuprizone-induced demyelination. *Brain Pathol*. 13:329–339.

van Luijtelaar G, Zobeiri M. 2014. Progress and outlooks in a genetic absence epilepsy model (WAG/Rij). *Curr Med Chem*. 21:704–721.

van Luijtelaar G, Lyashenko S, Vastyanov R, Verbeek G, Oleinik A, Van Rijn C, Volokhova G, Shandra A, Coenen A, Godlevsky L. 2012. Cytokines and absence seizures in a genetic rat model. *Neurophysiology*. 43:478–486.

Wachsmuth L, Datunashvili M, Kemper K, Albers F, Lambers H, Lüttjohann A, Kreitz S, Budde T, Faber C. 2021. Retrosplenial cortex contributes to network changes during seizures in the GAERS absence epilepsy rat model. *Cereb Cortex Commun*. 2:1–16.

Wahl-Schott C, Biel M. 2009. HCN channels: structure, cellular regulation and physiological function. *Cell Mol Life Sci* 66:470–494.

Wilkars W, Liu Z, Lewis AS, Stoub TR, Ramos EM, Brandt N, Nicholson DA, Chetkovich DM, Bender RA. 2012. Regulation of axonal

HCN1 trafficking in perforant path involves expression of specific TRIP8b isoforms. *PLoS One*. 7:e32181.

Yan B, Li P. 2013. The emergence of abnormal hypersynchronization in the anatomical structural network of human brain. *NeuroImage*. 65:34–51.

Yuan A, Rao M V., Veeranna, Nixon RA. 2012. Neurofilaments at a glance. *J Cell Sci*. 125:3257–3263.

Yue BW, Huguenard JR. 2001. The role of H-current in regulating strength and frequency of thalamic network oscillations. *Thalamus Relat Syst*. 1:95–103.

Zendedel A, Beyer C, Kipp M. 2013. Cuprizone-induced demyelination as a tool to study remyelination and axonal protection. *J Mol Neurosci*. 51:567–572.

Zhan J, Mann T, Joost S, Behrangi N, Frank M, Kipp M. 2020. The cuprizone model: dos and do nots. *Cell*. 9:843.

Zhao R, Zhou H, Su SB. 2013. A critical role for interleukin-1β in the progression of autoimmune diseases. *Int Immunopharmacol*. 17:658–669.

Zhu X, Yao Y, Hu Y, Yang J, Zhang C, He Y, Zhang A, Liu X, Zhang C, Gan G. 2021. Valproic acid suppresses cuprizone-induced hippocampal demyelination and anxiety-like behavior by promoting cholesterol biosynthesis. *Neurobiol Dis*. 158: 105489

Zobeiri M, Chaudhary R, Datunashvili M, Heuermann RJ, Lüttjohann A, Narayanan V, Balfanz S, Meuth P, Chetkovich DM, Pape H-C, et al. 2018. Modulation of thalamocortical oscillations by TRIP8b, an auxiliary subunit for HCN channels. *Brain Struct Funct*. 223: 1537–1564.

Zobeiri M, Chaudhary R, Blaich A, Rottmann M, Herrmann S, Meuth P, Bista P, Kanyshkova T, Lüttjohann A, Narayanan V, et al. 2019. The hyperpolarization-activated HCN4 channel is important for proper maintenance of oscillatory activity in the thalamocortical system. *Cereb Cortex*. 29:2291–2304.

Zobeiri M, van Luijtelaar G, Budde T, Sysoev IV. 2019. The brain network in a model of thalamocortical dysrhythmia. *Brain Connect*. 9: 273–284.

Zoupi L, Booker SA, Eigel D, Werner C, Kind PC, Spires-Jones TL, Newland B, Williams AC. 2021. Selective vulnerability of inhibitory networks in multiple sclerosis. *Acta Neuropathol*. 141: 415–429.